

# Thinking with Deltas: Incentivizing Reinforcement Learning via Differential Visual Reasoning Policy

Shujian Gao<sup>1</sup>, Yuan Wang<sup>2</sup>, Jiangtao Yan<sup>3</sup>, Zuxuan Wu<sup>1,†</sup>, Yu-Gang Jiang<sup>1,†</sup>

<sup>1</sup>Fudan University <sup>2</sup>Zhejiang University <sup>3</sup>Wuhan University

## Abstract

Reinforcement Learning with Verifiable Rewards (RLVR) has significantly advanced reasoning capabilities in Large Language Models. However, adapting RLVR to multimodal domains suffers from a critical *perception-reasoning decoupling*. Existing paradigms, driven by text-centric outcome rewards, reasoning in language medium, inadvertently encourage models to bypass visual perception. We empirically validate this through blind experiments: state-of-the-art policies maintain or surprisingly improve performance even when visual inputs are entirely removed. This reveals that these models degenerate into *blind reasoners*, exploiting linguistic priors to generate plausible answers instead of attending to visual evidence. In response, we propose **Thinking with Deltas**, a framework driven by a **Differential Visual Reasoning Policy (DVRP)**. DVRP introduces intrinsic supervision via visual triplets, comprising original, masked, and perturbed inputs. It optimizes the model to maximize reasoning divergence from masked inputs (enforcing *visual sensitivity*) while minimizing divergence from perturbed inputs (ensuring *visual robustness*). By aligning reasoning variations strictly with the *Delta* of visual information, DVRP inherently bolsters visual understanding capabilities and significantly outperforms state-of-the-art methods on both general and medical benchmarks, without requiring external annotations or auxiliary tools.

## 1 Introduction

Recent advancements in Large Language Models (LLMs) (Chang et al., 2024; Brown et al., 2020) have been substantially driven by Chain-of-Thought (CoT) prompting and the curation of high-quality reasoning data (Kojima et al., 2022; Ye et al., 2025). Building on this foundation, Reinforcement Learning with Verifiable Rewards

(RLVR) (Ouyang et al., 2022; Shao et al., 2024) has emerged as a promising post-training paradigm. By incentivizing self-correction and scaling test-time compute, RLVR enables models to generate rigorous and self-consistent solution paths, establishing a new standard for complex problem-solving in textual domains (Wang et al., 2025e).

However, a fundamental misalignment arises when directly applying the RLVR paradigm to multimodal domains (Liu et al., 2025a). Predominant approaches typically mirror text-centric methodologies (DeepSeek-AI et al., 2025) and rely heavily on textual outcome rewards such as accuracy or format constraints (Wang et al., 2025f). Furthermore, attempts to incorporate process supervision via external judges often inherit the biases and limitations of the judge models themselves (Luo et al., 2025). Conceptually, if we analogize a Multimodal LLM (MLLM) to a human observer, the visual encoder functions as the eyes. Optimizing rewards based solely on the output text sequence is equivalent to evaluating speech without verifying vision. This approach neither ensures the effective perception of visual signals nor stimulates deep visual understanding (Han et al., 2025b). Consequently, current frameworks neglect the causal dependency between visual inputs and reasoning outcomes.

As illustrated in Figure 1, we empirically validate this decoupling through **blind experiments** where visual inputs are either removed (Text Only) or replaced with blank images (Black/White). We investigate the behaviors of DAPO and GRPO under varying input configurations. For the GRPO baseline (Shao et al., 2024), the observed performance drop is negligible. This result is counter-intuitive, as the absence of essential visual contexts should theoretically precipitate a substantial performance collapse. Even more strikingly, DAPO (Yu et al., 2025) exhibits an *unexpected performance gain*: removing visual information *improves* accuracy (e.g., **+3.5%** on MathVista). These find-

<sup>†</sup>Corresponding authors.

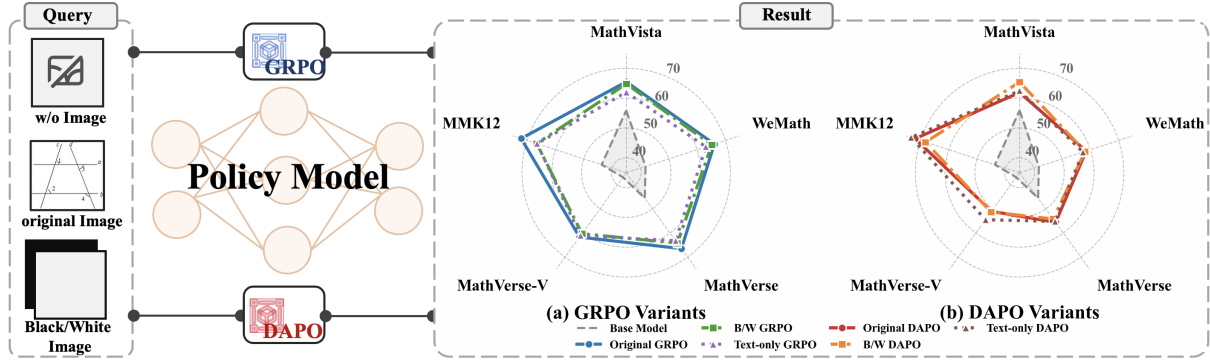


Figure 1: **Empirical Validation of Visual Decoupling.** Performance comparison in blind settings (Text Only or Blank Image) reveals latent reward hacking. The negligible performance drop in GRPO and the *unexpected performance gain* in DAPO (where removing visual inputs actually improves accuracy) indicate that policies degenerate into *blind reasoners* relying on linguistic shortcuts rather than visual evidence.

ings suggest distinct *reward hacking*, where the policy degenerates into a *blind reasoner*. Rather than grounding reasoning in visual perception, the model exploits linguistic shortcuts to maximize rewards, effectively treating visual data as distractive noise rather than indispensable evidence (Detailed analysis in Section E).

To address this perception-reasoning decoupling without resorting to complex data construction (Liu et al., 2024a) or external reward engineering (Zhang et al., 2025d), we propose **Thinking with Deltas**, a novel framework centered around a **Differential Visual Reasoning Policy (DVRP)**. Rather than relying on proxy textual rewards, DVRP introduces intrinsic visual supervision by constructing a visual triplet input stream: (1) *Invariant* (the original image), (2) *Decremental* (masked visual input), and (3) *Incremental* (perturbed visual input). Our core insight is that genuine visual reasoning must be strictly sensitive to the *Delta* ( $\Delta$ ) of visual information. Specifically, DVRP enforces a differential policy that maximizes the divergence between the *Invariant* and *Decremental* states (proving visual sensitivity) while minimizing the divergence between the *Invariant* and *Incremental* states (ensuring visual robustness). By optimizing these differential signals end-to-end, DVRP effectively compels the model to attend to visual evidence without requiring expensive external tools or dense annotations.

Our contributions are summarized as follows:

- We identify the perception-reasoning decoupling in current multimodal RL as a primary bottleneck, arguing that standard objectives optimize for linguistic plausibility rather than

visual grounding.

- We introduce the **DVRP**, an algorithm that leverages visual triplets to construct intrinsic *Delta supervision signals* for both visual sensitivity and robustness, inherently bolstering visual perception and reasoning capabilities.
- Extensive experiments spanning domains from **general mathematical reasoning** to **specialized medical diagnostics** demonstrate that DVRP significantly outperforms state-of-the-art RLVR methods like GRPO (Shao et al., 2024) and DAPO (Yu et al., 2025), effectively enhancing visual perception capabilities.

## 2 Related Work

### 2.1 Multimodal Reasoning

Recent advancements in Multimodal Large Language Models (MLLMs) have significantly extended the reasoning capabilities of LLMs to visual domains (Wang et al., 2024a). Pioneering works such as LLaVA (Liu et al., 2024a) and Qwen-VL (Bai et al., 2023) demonstrated that visual instruction tuning could effectively align visual encoders with LLMs, enabling strong performance on general visual-oriented benchmarks (Yue et al., 2024b). Following this, the community has focused on enhancing the reasoning depth of these models. Inspired by the efficacy of CoT in LLMs, the integration of Multimodal-CoT (Zhang et al., 2024c; Sarch et al., 2025) and the curation of high-quality reasoning datasets (Chen et al., 2024b, 2023; Dong et al., 2025; Sun et al.) have emerged as pivotal strategies for bolstering visual understanding,

thereby significantly mitigating linguistic hallucinations (Huang et al., 2024; Leng et al., 2024).

To substantially enhance visual understanding, a novel paradigm, which termed *visual reasoning in action* has emerged, advocating for thinking with images by explicitly incorporating visual content within CoT processes (Su et al., 2025). Representative strategies employ visual programming via code generation (Surís et al., 2023; Gupta and Kembhavi, 2023; Lin et al., 2025), leverage external visual utilities (e.g., crop, zoom, rotate) (Zheng et al., 2025b; Zhang et al., 2025a; Qi et al., 2024; Liu et al., 2023), or orchestrate diverse expert models to tackle multimodal tasks (Shen et al., 2023; Lu et al., 2023). Further explorations extend to tool-integrated, multi-turn, and multi-agent system for interleaved reasoning (Wu et al., 2025; Chen et al., 2024c; Wang et al., 2025b; Man et al., 2025) and unified frameworks (Han et al., 2025a; Li et al., 2025a). *However, these methods rely heavily on external sources such as expensive trajectory data, agentic tools, or advanced teacher models. This incurs significant overhead and does not fundamentally improve the model’s intrinsic visual perception and reasoning capabilities.*

## 2.2 Advancements in RLVR Frameworks

Recent research on RLVR focuses on optimizing three critical components: **Data**, **Reward**, and **Rollout**.

**Data Curation.** High-quality Chain-of-Thought initialization is a prerequisite for stable RL training (Chen et al., 2025b; Huang et al., 2025a; Zhang et al., 2025c; Liang et al., 2025). Complementing this, recent studies employ dynamic data selection strategies, such as filtering trajectories based on value estimation (Wang et al., 2025d) or applying perplexity- and difficulty-based correction mechanisms (Kong et al., 2024; Jiang et al., 2025) to enhance sample efficiency and diversity.

**Reward Engineering.** Granular reward design serves as a pivotal mechanism in RLVR (DeepSeek-AI et al., 2025). Dominant approaches rely on *outcome-based* signals, including rigorous accuracy verification (Liu et al., 2025b), strict formatting and length constraints (Parthasarathi et al., 2025; Zhang and Zuo, 2025), caption alignment metrics (Gou et al., 2025b) for visual-semantic understanding, and grounding constraints (Zhang et al., 2025d). To further mitigate reasoning shortcuts, recent methods augment these with *process-level constraints* (Jiang et al., 2025), aiming to bol-

ster the procedural correctness and reliability of intermediate reasoning chains.

**Rollout Optimization.** Enhancing the efficiency of the exploration phase is another active frontier. Recent strategies focus on optimizing the rollout space by dynamically adjusting sampling temperatures (Liao et al., 2025), expanding the sampling space (Liu et al., 2025a; Li et al., 2025b), polishing reasoning processes (Fan et al., 2025), and employing tree-search algorithms to diversify generation paths (Ji et al., 2025). These methods aim to balance exploration and exploitation, ensuring the policy covers a broader solution space without diverging into incoherence.

*However, these strategies relegate the visual modality to an auxiliary role relative to text, neglecting the critical need to enhance visual robustness and sensitivity in MLLMs. In contrast, our proposed DVRP intrinsically fosters the model’s visual perception capabilities.*

## 3 Method

### 3.1 Problem Formulation

**Preliminaries on GRPO.** We consider a multimodal reasoning task where a policy model  $\pi_\theta$ , parameterized by  $\theta$ , takes a visual input  $I$  and a textual query  $q$  to generate a reasoning chain followed by a final answer, denoted as  $o$ . The training dataset is represented as  $\mathcal{D} = \{(I, q, a)\}$ , where  $a$  is the ground truth answer.

Recent advancements in RLVR have largely adopted GRPO (Shao et al., 2024) to enhance reasoning capabilities without the need for a separate value network. Formally, for each input instance  $(I, q)$ , GRPO samples a group of  $G$  outputs  $\{o_i\}_{i=1}^G$  from the old policy  $\pi_{\theta_{old}}$ . A rule-based reward function  $r(o, a)$  evaluates the correctness of each output (e.g., format compliance and answer accuracy), assigning a reward  $R_i$ . To reduce variance, the advantage  $\hat{A}_i$  for the  $i$ -th output is computed by normalizing the rewards within the group:

$$\hat{A}_i = \frac{R_i - \text{mean}(\{R_j\}_{j=1}^G)}{\text{std}(\{R_j\}_{j=1}^G) + \epsilon}, \quad (1)$$

where  $\epsilon$  is a small constant for numerical stability. The optimization objective of GRPO is defined as:

$$\mathcal{J}_{\text{GRPO}}(\theta) = \mathbb{E}_{q \sim \mathcal{D}, \{o_i\} \sim \pi_{\theta_{old}}} \left[ \frac{1}{G} \sum_{i=1}^G \mathcal{L}_{\text{clip}}(o_i, \hat{A}_i) \right], \quad (2)$$

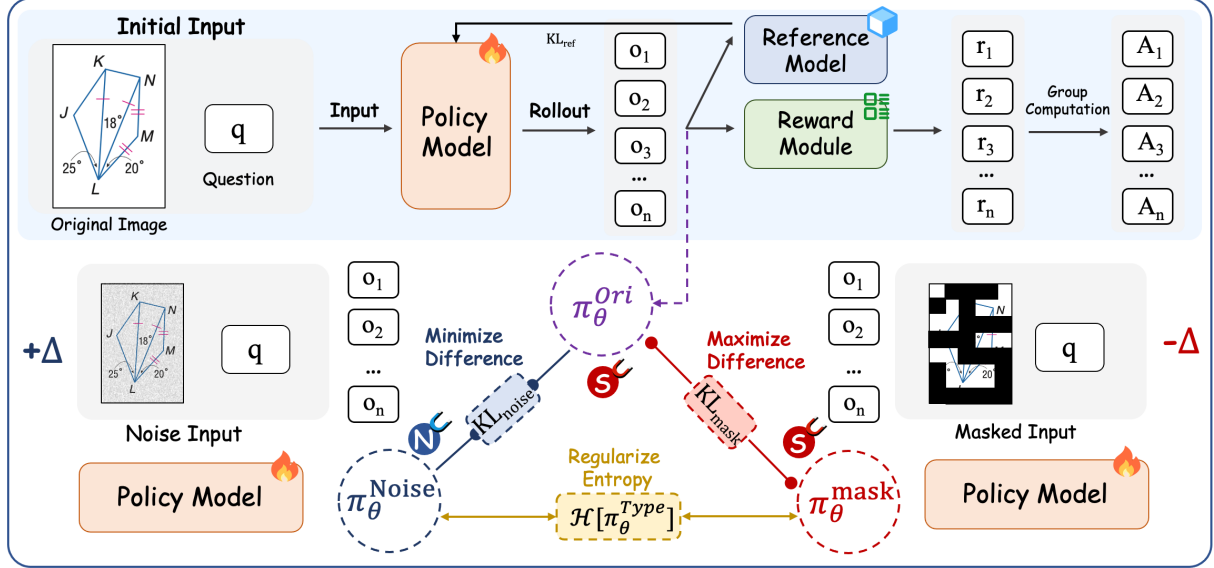


Figure 2: The framework of DVRP. Our method bridges the perception-reasoning decoupling via a visual triplet contrastive learning objective. The upper stream represents the standard reasoning rollout. The lower streams enforce two critical visual properties: (1) Visual Robustness: minimizing the KL-divergence ( $KL_{noise}$ ) between predictions on original and noise-perturbed inputs ( $+\Delta$ ); and (2) Visual Sensitivity: maximizing the divergence ( $KL_{mask}$ ) when critical visual semantics are occluded ( $-\Delta$ ). An entropy regularization term  $\mathcal{H}$  prevents distribution collapse.

where  $\mathcal{L}_{clip}$  denotes the standard PPO clipped surrogate loss:

$$\mathcal{L}_{clip} = \min \left( \rho_i \hat{A}_i, \text{clip}(\rho_i, 1 - \epsilon_{clip}, 1 + \epsilon_{clip}) \hat{A}_i \right), \quad (3)$$

with  $\rho_i = \frac{\pi_\theta(o_i|I,q)}{\pi_{\theta,old}(o_i|I,q)}$  representing the probability ratio. Following recent practices (Yu et al., 2025), we remove the KL divergence penalty term to encourage sufficient exploration.

**The Perception-Reasoning Decoupling.** A critical limitation of current multimodal RLVR paradigms is their failure to enforce the *causal dependency* between visual perception and reasoning paths (Jiang et al., 2025). By relying solely on outcome-based textual rewards and reasoning in language medium, these methods treat visual inputs as optional context rather than necessary evidence. Consequently, existing frameworks largely overlook the model’s **sensitivity to critical visual semantics** and **robustness against visual perturbations**, inadvertently incentivizing linguistic shortcuts over visually grounded reasoning (Han et al., 2025b).

### 3.2 Visual Triplets as Intrinsic Supervision

To bridge this gap, we propose **DVRP**, which introduces intrinsic supervision via a *Visual Triplet* mechanism. As illustrated in Figure 2, for each training instance, we construct three distinct views:

- **Invariant View ( $I$ ):** The original visual input, serving as the anchor for standard reasoning. The policy distribution under this view is denoted as  $\pi_\theta^{Ori} = \pi_\theta(\cdot|I, q)$ .
- **Decremental View ( $I_{mask}$ ):** A “ $-\Delta$ ” state generated by masking visual regions randomly. This creates a counterfactual scenario where visual evidence is lost. The corresponding policy is  $\pi_\theta^{Mask} = \pi_\theta(\cdot|I_{mask}, q)$ .
- **Incremental View ( $I_{noise}$ ):** A “ $+\Delta$ ” state generated by injecting non-semantic Diffusion noise. This simulates environmental instability while preserving semantics. The corresponding policy is  $\pi_\theta^{Noise} = \pi_\theta(\cdot|I_{noise}, q)$ .

This triplet structure allows us to operationalize two complementary learning signals: *Visual Sensitivity* (diverging from  $\pi_\theta^{Mask}$ ) and *Visual Robustness* (aligning with  $\pi_\theta^{Noise}$ ). We conducted comprehensive experiments to investigate the insights and applicability of our approach, which are detailed in Section D.

### 3.3 Optimization Objective

Formally, DVRP optimizes a unified objective that balances task performance with intrinsic visual grounding. We integrate visual triplet supervision into the GRPO framework to **enforce** two complementary constraints: (1) **Visual Sensitivity**: The

Method	General Multimodal Reasoning							Medical Multimodal Reasoning						Overall		
	Geo3k	Vista	WeMath	MVerse	MVerse-V	MMKI2	AVG	$\Delta_{rel}$	Slake	Path	Rad	PMC	AVG	$\Delta_{rel}$	AVG	$\Delta_{rel}$
<i>Qwen2.5-VL-3B Backbone</i>																
<b>Base Model</b>	20.6	40.6	23.9	30.9	28.2	34.8	29.8	<i>Ref.</i>	48.7	59.2	40.3	46.8	48.7	<i>Ref.</i>	37.4	<i>Ref.</i>
GRPO	28.7	59.3	58.9	55.3	52.2	57.2	51.9	$\uparrow 44.2\%$	70.9	74.5	71.2	53.4	67.5	$\uparrow 38.6\%$	58.2	$\uparrow 55.6\%$
DAPO	31.2	60.9	60.0	56.3	53.0	<b>66.8</b>	54.7	$\uparrow 83.6\%$	71.3	72.4	70.8	56.6	67.8	$\uparrow 39.2\%$	59.9	$\uparrow 60.2\%$
NoiseRollout	32.5	63.0	60.1	56.9	53.5	63.4	54.9	$\uparrow 84.2\%$	72.5	76.1	75.0	61.0	71.2	$\uparrow 46.2\%$	61.4	$\uparrow 64.2\%$
PAPO	30.9	61.3	60.1	57.1	53.9	57.3	53.4	$\uparrow 79.2\%$	72.1	75.9	74.8	60.7	70.9	$\uparrow 45.6\%$	60.4	$\uparrow 61.5\%$
<b>DVRP<sub>D</sub> (Ours)</b>	<b>35.1</b>	64.9	<b>60.5</b>	<b>58.1</b>	<b>54.8</b>	60.9	<b>55.7</b>	$\uparrow 86.9\%$	76.3	<b>78.9</b>	75.9	<b>62.2</b>	<b>73.3</b>	$\uparrow 50.5\%$	62.7	<b>167.6\%</b>
<b>DVRP<sub>G</sub> (Ours)</b>	34.5	<b>65.5</b>	60.3	57.7	54.5	61.2	55.6	$\uparrow 86.6\%$	<b>74.1</b>	77.5	<b>76.2</b>	61.5	72.3	$\uparrow 48.5\%$	62.3	$\uparrow 66.6\%$
<i>Qwen2.5-VL-7B Backbone</i>																
<b>Base Model</b>	33.8	55.9	41.8	45.6	36.9	43.7	43.0	<i>Ref.</i>	63.7	60.6	61.3	52.2	59.5	<i>Ref.</i>	49.6	<i>Ref.</i>
GRPO	40.2	65.5	66.1	66.5	61.7	72.1	62.0	$\uparrow 44.2\%$	74.7	75.7	74.9	56.2	70.4	$\uparrow 18.3\%$	65.4	$\uparrow 31.9\%$
DAPO	35.9	61.9	58.5	55.6	51.0	71.9	55.8	$\uparrow 29.8\%$	74.9	76.2	67.8	57.2	69.0	$\uparrow 16.0\%$	61.1	$\uparrow 23.2\%$
NoiseRollout	39.7	67.8	65.3	66.1	62.8	70.5	62.0	$\uparrow 44.2\%$	72.8	74.1	72.2	59.9	69.8	$\uparrow 17.3\%$	65.1	$\uparrow 31.3\%$
PAPO	40.2	69.5	66.7	68.4	64.9	72.5	63.7	$\uparrow 48.1\%$	76.9	73.4	77.5	61.6	72.4	$\uparrow 21.7\%$	67.2	$\uparrow 35.5\%$
<b>DVRP<sub>D</sub> (Ours)</b>	<b>43.4</b>	70.9	67.8	<b>68.9</b>	65.3	74.1	65.1	$\uparrow 51.4\%$	80.3	<b>79.7</b>	<b>80.5</b>	64.2	76.2	$\uparrow 28.1\%$	69.5	$\uparrow 40.1\%$
<b>DVRP<sub>G</sub> (Ours)</b>	42.3	<b>71.1</b>	<b>68.1</b>	67.4	<b>66.7</b>	<b>75.6</b>	<b>65.2</b>	$\uparrow 51.6\%$	<b>81.7</b>	78.3	79.9	<b>65.5</b>	<b>76.4</b>	$\uparrow 28.4\%$	69.7	$\uparrow 40.5\%$

Table 1: Performance (avg@8 acc %) comparison of Qwen2.5-VL-3B and 7B backbones. We compare our **DVRP** against baselines including GRPO, DAPO, and PAPO. Subscripts  $D$  and  $G$  denote optimizations using DAPO and GRPO, respectively. The **Base Model** (highlighted) serves as the reference for calculating relative improvements ( $\Delta_{rel} = \frac{\text{Method} - \text{Base}}{\text{Base}} \times 100\%$ ). For a fair comparison, all baselines are reproduced in the same environment and evaluated using the identical suite.

policy must diverge from the decremental view ( $\pi_\theta^{Mask}$ ) where visual evidence is absent; (2) **Visual Robustness**: The policy must remain consistent with the incremental view ( $\pi_\theta^{Noise}$ ) despite perturbations.

However, directly constraining the consistency in the robustness and sensitivity branches can lead to a degenerate solution where the policy collapses into a high-entropy uniform distribution to trivially minimize the KL divergence. To mitigate this risk, we incorporate an entropy regularization term to penalize high uncertainty, preventing the model from converging to such a trivial state. Consequently, the final optimization objective  $\mathcal{J}_{\text{DVRP}}$  is formulated as:

$$\begin{aligned} \mathcal{J}_{\text{DVRP}}(\theta) = & \underbrace{\mathcal{J}_{\text{GRPO}}(\theta)}_{\text{Maximize Reward}} \\ & + \lambda_{nec} \cdot \mathbb{D}_{KL} \left( \pi_\theta^{Ori} \parallel \pi_\theta^{Mask} \right) \\ & \underbrace{\quad \quad \quad \text{Visual Sensitivity} \quad (\text{Max Difference})}_{\quad \quad \quad} \\ & - \lambda_{rob} \cdot \mathbb{D}_{KL} \left( \pi_\theta^{Ori} \parallel \pi_\theta^{Noise} \right) \\ & \underbrace{\quad \quad \quad \text{Visual Robustness} \quad (\text{Min Difference})}_{\quad \quad \quad} \\ & - \lambda_{ent} \cdot \mathbb{E} \left[ \mathcal{H}(\pi_\theta^{Noise}) + \mathcal{H}(\pi_\theta^{Mask}) \right], \\ & \underbrace{\quad \quad \quad \text{Entropy Penalty} \quad (\text{Prevent Collapse})}_{\quad \quad \quad} \end{aligned} \quad (4)$$

where  $\pi_{\theta_{old}}$  (implicitly used in  $\mathcal{J}_{\text{GRPO}}$ ) serves as the frozen reference distribution to stabilize the reward maximization, while the triplet objectives enforce constraints on the current policy manifold.

## 4 Experiments

### 4.1 Experiment Setup and Training Details

**Implementation Framework.** Our experimental framework is built upon Easy-R1 (Zheng et al., 2025a), implemented using Python 3.10 and PyTorch 2.4.0 (Paszke et al., 2019) with CUDA 12.4 support. Following the training paradigm established by DeepSeek-R1 (DeepSeek-AI et al., 2025), we employed Direct Reinforcement Fine-Tuning (RFT) to optimize the Qwen2.5-VL-7B and 3B backbones (Qwen et al., 2025). All experiments were conducted on a computational cluster equipped with 4× NVIDIA A800 GPUs.

**Training Datasets.** To foster robust reasoning across domains, we employ ViRL39K (Wang et al., 2025a) for mathematical training, while for the medical domain, we construct a composite dataset by amalgamating the training splits of Slake (Liu et al., 2021), PathVQA (He et al., 2020), Rad-VQA (Lau et al., 2018), and PMC-VQA (Zhang et al., 2024b).

**Training Details.** To demonstrate the versatility of the proposed **DVRP**, we integrated DVRP with two fundamental RLVR algorithms, DAPO (Yu et al., 2025) and GRPO (Shao et al., 2024), and evaluated its impact on the Qwen2.5-VL-7B and 3B backbones (Qwen et al., 2025). We conducted extensive ablation studies to determine the optimal masking ratios and noise levels (Jiang et al., 2025). Details are provided in Appendix C. Following the methodology of NoiseRollout (Liu et al., 2025a),

Method	In-Domain Datasets				Out-of-Domain Datasets	
	PMCVQA	VQA-RAD	SLAKE	PathVQA	MedXpertQA	MMMU-Med
<i>Proprietary Models</i>						
Gemini-2.0-flash-lite	50.8	59.4	73.1	64.9	–	58.7
GPT-4.1-Nano	53.1	61.8	73.1	70.6	–	60.6
GPT-4o	–	63.9	71.6	75.9	–	–
<i>General-purpose Multimodal VLMs</i>						
Qwen-VL-Chat (Wang et al., 2024b)	36.6	47.0	56.0	55.1	–	32.7
Yi-VL-34B (AI et al., 2025)	39.5	53.0	58.9	47.3	–	41.5
LLaVA-v1.6-7B (Liu et al., 2024b)	35.5	52.6	57.9	47.9	–	33.1
LLaVA-v1.6-13B (Liu et al., 2024b)	36.6	55.8	58.9	51.9	–	39.3
LLaVA-v1.6-34B (Liu et al., 2024b)	44.4	58.6	67.3	59.1	–	48.8
LLaVA-v1.5-LLaMA3-8B (Contributors, 2023)	36.4	54.2	59.4	54.1	–	38.2
<i>Medical Multimodal VLMs</i>						
Med-Flamingo (Moor et al., 2023)	23.3	45.4	43.5	54.7	22.1	28.3
RadFM (Wu et al., 2023)	25.9	50.6	34.6	38.7	23.4	27.0
LLaVA-Med-7B (Li et al., 2023)	24.7	51.4	48.6	56.8	20.8	36.9
LLaVA_Med-LLaMA3-8B (Contributors, 2023)	46.6	60.2	61.2	54.5	–	41.1
PubMedVision-8B (Chen et al., 2024a)	52.7	63.8	74.5	59.9	–	49.1
HuatuoGPT-Vision-34B (Chen et al., 2024a)	58.2	68.1	76.9	63.5	22.1	54.4
MedVLThinker-7B (Huang et al., 2025b)	57.5	63.7	67.8	65.2	20.9	57.0
CAPO-7B (Jiang et al., 2025)	55.5	78.5	79.1	68.9	–	60.0
<i>Medical Agentic Systems</i>						
MedAgents (Tang et al., 2024)	–	65.6	67.9	63.2	–	49.7
MDAgents (Kim et al., 2024)	–	66.8	68.2	65.4	–	52.3
AFlow (Zhang et al., 2025b)	–	67.3	68.9	66.4	–	53.6
MMedAgent-RL-7B (Xia et al., 2025)	–	71.5	76.2	72.3	–	<b>66.4</b>
<i>Ours</i>						
<b>Base Model (Qwen2.5-VL-3B)</b>	46.8	40.3	48.7	59.2	20.7	31.5
+ DVRP <sub>G</sub>	61.5	76.2	74.1	77.5	23.2	42.4
	<b>+14.7</b>	<b>+35.9</b>	<b>+25.4</b>	<b>+18.3</b>	<b>+2.5</b>	<b>+10.9</b>
+ DVRP <sub>D</sub>	62.2	75.9	76.3	<u>78.9</u>	<u>24.1</u>	44.1
	<b>+15.4</b>	<b>+35.6</b>	<b>+27.6</b>	<b>+19.7</b>	<b>+3.4</b>	<b>+12.6</b>
<b>Base Model (Qwen2.5-VL-7B)</b>	52.2	61.3	63.7	60.6	20.1	54.7
+ DVRP <sub>G</sub>	<b>65.5</b>	<u>79.9</u>	<b>81.7</b>	78.3	24.0	<b>66.2</b>
	<b>+13.3</b>	<b>+18.6</b>	<b>+18.0</b>	<b>+17.7</b>	<b>+3.9</b>	<b>+11.5</b>
+ DVRP <sub>D</sub>	64.2	<b>80.5</b>	80.3	<b>79.7</b>	<b>25.7</b>	65.9
	<b>+12.0</b>	<b>+19.2</b>	<b>+16.6</b>	<b>+19.1</b>	<b>+5.6</b>	<b>+11.2</b>

Table 2: Comprehensive performance comparison on 2D medical VQA benchmarks. **Bold** and underline denote best and second-best scores. The green values indicate the absolute improvement over the corresponding Base Model. Subscripts  $D$  and  $G$  denote optimizations using DAPO and GRPO, respectively.

we adopted a sigmoid function for diffusion noise annealing (Detailed in Section B.4). We also adopt random patch masking as the visual sensitivity operation in this work, a choice that has been discussed in (Wang et al., 2025g). Specifically, the KL divergence terms are computed as the summation of **token-level KL divergences** between the categorical output distributions of the compared policies at each generation step, calculated over the trajectories sampled from the invariant policy  $\pi_\theta^{Ori}$ . Detailed hyperparameter configurations are provided in Appendix B.2.

**Evaluation Protocol.** We conduct a comprehensive evaluation across benchmarks spanning both in-domain and out-of-domain settings. Our comparative analysis includes a wide range of baselines, comprising closed-source commercial models, open-source general-purpose models, and domain-specific reasoning models. For detailed experimental settings, please refer to Section B.1

## 4.2 Main Experiments

### 4.2.1 RLVR Experiments

We benchmark DVRP against representative RLVR baselines (Liu et al., 2025a) (Table 1). On the

Method	Mathematical Multimodal Reasoning						
	Geo3k	Vista	WeMath	MVerse	MVerse-V	MMKI2	AVG
<i>Proprietary Models</i>							
GPT-4o	–	64.7	62.8	50.2	53.8	55.8	57.5
GPT-4o-mini	–	59.9	56.3	42.3	45.1	51.9	51.1
Gemini-2.0-flash	–	70.4	47.4	47.8	48.7	65.2	55.9
<i>General-purpose Multimodal VLMs</i>							
Qwen2.5-VL-72B (Wang et al., 2024b)	–	<b>74.2</b>	49.1	47.3	48.6	70.5	57.9
InternVL2.5-8B (Chen et al., 2025c)	–	64.9	44.9	37.0	40.2	46.8	46.8
InternVL2.5-VL-78B (Chen et al., 2025c)	–	64.9	44.9	37.0	40.2	59.8	49.4
LLaVA-OneVision-7B (Li et al., 2024)	–	58.5	44.1	–	–	–	51.3
LLaVA-OneVision-72B (Li et al., 2024)	–	67.1	32.0	27.2	30.1	–	39.1
LLaVA-OneVision-1.5-8B (An et al., 2025)	–	69.6	61.5	–	–	–	<b>65.6</b>
LLaVA-Critic-R1-7B (Wang et al., 2025c)	35.4	68.7	62.6	58.9	53.1	57.4	56.0
R1-OneVision-7B (Yang et al., 2025)	30.6	64.9	55.2	61.7	44.3	43.3	50.0
<i>Math-Specific Multimodal VLMs</i>							
MM-Eureka-7B (Meng et al., 2025a)	36.4	59.1	45.3	57.6	56.4	60.6	52.6
MM-Eureka-7B-CPGD (Liu et al., 2025c)	37.6	64.2	64.3	63.7	59.2	64.7	59.0
ADORA-7B (Gui and Ren, 2025)	41.2	61.1	53.0	45.2	41.8	49.8	48.7
R1-VL-7B (Zhang et al., 2025c)	31.9	63.5	56.1	42.0	43.2	55.3	48.7
VLAAThinker-7B (Chen et al., 2025a)	24.2	67.4	65.9	47.9	52.0	63.2	53.4
VL-Rethinker-7B (Wang et al., 2025a)	33.6	61.3	66.5	64.0	60.8	59.8	57.7
RACRO-7B-CRO-GRPO (Gou et al., 2025b)	41.4	61.7	<b>68.9</b>	65.7	61.7	70.5	61.7
ThinkLite-7B-VL (Wang et al., 2025d)	34.4	68.9	63.5	49.5	46.0	56.2	53.1
<i>Ours</i>							
<b>Base Model</b> (Qwen2.5-VL-3B)	20.6	40.6	23.9	30.9	28.2	34.8	29.8
+ DVRP <sub>D</sub>	35.1	64.9	60.5	58.1	54.8	60.9	55.7
	<b>+14.5</b>	<b>+24.3</b>	<b>+36.6</b>	<b>+27.2</b>	<b>+26.6</b>	<b>+26.1</b>	<b>+25.9</b>
+ DVRP <sub>G</sub>	34.5	65.5	60.3	57.7	54.5	61.2	55.6
	<b>+13.9</b>	<b>+24.9</b>	<b>+36.4</b>	<b>+26.8</b>	<b>+26.3</b>	<b>+26.4</b>	<b>+25.8</b>
<b>Base Model</b> (Qwen2.5-VL-7B)	33.8	55.9	41.8	45.6	36.9	43.7	43.0
+ DVRP <sub>D</sub>	<b>43.4</b>	70.9	67.8	<b>68.9</b>	<b>65.3</b>	<b>74.1</b>	65.1
	<b>+9.6</b>	<b>+15.0</b>	<b>+26.0</b>	<b>+23.3</b>	<b>+28.4</b>	<b>+30.4</b>	<b>+22.1</b>
+ DVRP <sub>G</sub>	<b>42.3</b>	<b>71.1</b>	<b>68.1</b>	<b>67.4</b>	<b>66.7</b>	<b>75.6</b>	65.2
	<b>+8.5</b>	<b>+15.2</b>	<b>+26.3</b>	<b>+21.8</b>	<b>+29.8</b>	<b>+31.9</b>	<b>+22.2</b>

Table 3: Performance comparison on mathematical multimodal reasoning benchmarks. **Bold** and underline denote the best and second-best performance, respectively. The green values indicate the absolute improvement over the corresponding Base Model. Subscripts <sub>D</sub> and <sub>G</sub> denote optimizations using DAPO and GRPO, respectively.

7B scale, our approach consistently establishes new state-of-the-art results. Implementing DVRP on GRPO (DVRP<sub>G</sub>) yields an overall accuracy of 69.7%, representing a **40.5%** relative improvement over the base model and surpassing the strongest baseline PAPO by 2.5 points. In the medical domain, DVRP<sub>G</sub> reaches 76.4% accuracy with a relative gain of **28.4%**, demonstrating differential visual constraints effectively enhance robustness in specialized reasoning tasks. For further case studies and reasoning consistency evaluation, please

refer to Section G.

The performance gain is even more pronounced on the smaller 3B backbone. DVRP<sub>D</sub> boosts the overall accuracy from 37.4% to 62.7%, achieving a remarkable **67.6%** relative improvement. Crucially, our 3B model attains 73.3% on medical benchmarks, which surpasses the 70.4% accuracy of the significantly larger 7B GRPO baseline. These results validate that DVRP effectively compensates for limited model capacity by maximizing the utilization of visual evidence.

Method	General Multimodal Reasoning							Medical Multimodal Reasoning					Overall AVG
	Geo3k	Vista	WeMath	MVerse	MVerse-V	MMKI2	AVG	Slake	Path	Rad	PMC	AVG	
<i>Qwen2.5-VL-7B Backbone</i>													
Base Model (Original)	33.8	55.9	41.8	45.6	36.9	43.7	43.0	63.7	60.6	61.3	52.2	59.5	49.6
Baseline (GRPO)	40.2	65.5	66.1	66.5	61.7	72.1	62.0	74.7	75.7	74.9	56.2	70.4	65.4
+ Visual Sensitivity	41.5	68.8	67.2	<b>67.8</b>	64.8	73.9	64.0	78.5	<b>79.2</b>	78.2	61.4	74.3	68.1
+ Visual Robustness	40.9	67.2	66.6	67.0	63.2	73.0	63.0	76.2	76.5	<b>80.2</b>	59.1	73.0	67.0
<b>DVRP<sub>G</sub> (Full)</b>	<b>42.3</b>	<b>71.1</b>	<b>68.1</b>	67.4	<b>66.7</b>	<b>75.6</b>	<b>65.2</b>	<b>81.7</b>	78.3	79.9	<b>65.5</b>	<b>76.4</b>	<b>69.7</b>

Table 4: Ablation study of **Visual Sensitivity** (via masking) and **Visual Robustness** (via noise injection) on the Qwen2.5-VL-7B backbone. The **Base Model** (gray) represents the original pre-trained weights, while the **Baseline** utilizes the standard GRPO algorithm. While specific constraints (e.g., masking on PathVQA or noise on VQA-RAD) may yield marginal gains on individual datasets, the full **DVRP<sub>G</sub>** framework (green) achieves the best overall performance, demonstrating the synergy of the combined objectives.

#### 4.2.2 Domain Foundation Model Experiments

We evaluate DVRP against a wide spectrum of proprietary, general-purpose, and domain-specific foundation models across medical and mathematical benchmarks. In the medical domain, as detailed in Table 2, our 7B model establishes new state-of-the-art performance on in-domain tasks, consistently outperforming specialized baselines like CAPO-7B (Jiang et al., 2025) and HuatuoGPT-Vision-34B (Chen et al., 2024a). Notably, on PathVQA, DVRP<sub>D</sub> achieves **79.7%** accuracy, surpassing the proprietary GPT-4o score of 75.9% and rivaling complex agentic systems like MMedAgent-RL without requiring external tools or trajectory data (Zhang et al., 2025b).

Turning to the mathematical domain in Table 3, DVRP demonstrates superior generalization capabilities. Our 7B model attains an average accuracy of **65.2%**, significantly outperforming the 72B-parameter Qwen2.5-VL at 57.9% and GPT-4o at 57.5%. It also establishes a clear advantage over math-specific baselines such as RACRO-7B (Gou et al., 2025a) and MM-Eureka (Meng et al., 2025a), which score 61.7% and 59.0% respectively. These results indicate that by explicitly enforcing differential visual sensitivity and robustness, DVRP ensures consistent generalization across diverse datasets and model scales. Crucially, this approach empowers parameter-efficient models to rival or even exceed the reasoning capabilities of significantly larger counterparts and more sophisticated agentic reasoning systems (Xia et al., 2025).

#### 4.3 Ablation Experiments

To investigate the individual contributions of the proposed components, we conduct an ablation study on the Qwen2.5-VL-7B backbone using GRPO as the baseline (Table 4). The introduction

of *Visual Sensitivity* yields a substantial improvement over the baseline, confirming that penalizing blind reasoning is critical for enforcing genuine visual grounding. Similarly, the *Visual Robustness* term independently enhances performance by fostering stability against perturbations. While individual components may occasionally outperform the unified model on specific tasks, the full DVRP framework achieves the best overall performance. This demonstrates that sensitivity and robustness constraints are complementary, effectively synergizing to maximize reasoning reliability across diverse domains.

Furthermore, we explore the impact of perturbation intensity across domains. Our experiments reveal a domain-specific dichotomy: general multimodal reasoning (e.g., Math) benefits from aggressive perturbations ( $P_{mask} = 0.6, T_{init} = 500$ ) to enforce structural dependency, whereas medical reasoning requires milder regularization ( $P_{mask} = 0.2, T_{init} = 100$ ) to preserve fine-grained pathological features. We provide a detailed discussion of these hyperparameter sensitivities in Appendix C.

## 5 Conclusion

In this work, we address the critical perception-reasoning decoupling in current multimodal RLVR paradigms by proposing **Thinking with Deltas**. Driven by the **Differential Visual Reasoning Policy**, our framework leverages self-supervised **visual triplets** to introduce intrinsic supervision, compelling models to strictly align their reasoning with the presence and stability of visual evidence. This approach natively enhances perception without relying on external dependencies. Extensive experiments across mathematical and medical domains demonstrate that DVRP effectively bridges the perception-reasoning decoupling and empow-

ers parameter-efficient models (e.g., 3B and 7B) to achieve state-of-the-art performance, often rivaling significantly larger commercial baselines.

## Limitations

Despite the robust performance and generalization capabilities our method demonstrates across diverse domains and comparative settings, several limitations remain. First, our empirical evaluation is currently confined to models with 3B and 7B parameters. Due to computational resource constraints, we have not yet scaled the proposed framework to larger foundation models (e.g., 70B+ parameters) or verified its efficacy across a broader spectrum of architectural backbones. Consequently, the scalability of differential visual constraints on massive-scale models and their transferability to different model families remain to be fully characterized. Second, our current approach focuses on intrinsic policy optimization and has not yet explored integration with agentic systems. Synergizing DVRP with multi-agent frameworks or interactive tool-use pipelines to achieve more sophisticated reasoning strictly grounded on visual evidence remains an unexplored frontier. We hope this work inspires future research into differential constraints as a minimalist yet powerful paradigm for building trustworthy and visually grounded multimodal systems.

## References

01. AI, :, Alex Young, Bei Chen, Chao Li, Chengan Huang, Ge Zhang, Guanwei Zhang, Guoyin Wang, Heng Li, Jiangcheng Zhu, Jianqun Chen, Jing Chang, Kaidong Yu, Peng Liu, Qiang Liu, Shawn Yue, Senbin Yang, Shiming Yang, and 14 others. 2025. [Yi: Open foundation models by 01.ai](#). *Preprint*, arXiv:2403.04652.

Xiang An, Yin Xie, Kaicheng Yang, Wenkang Zhang, Xiuwei Zhao, Zheng Cheng, Yirui Wang, Songcen Xu, Changrui Chen, Chunsheng Wu, Huajie Tan, Chunyuan Li, Jing Yang, Jie Yu, Xiyao Wang, Bin Qin, Yumeng Wang, Zizhen Yan, Ziyong Feng, and 3 others. 2025. [Llava-onevision-1.5: Fully open framework for democratized multimodal training](#). *Preprint*, arXiv:2509.23661.

Jinze Bai, Shuai Bai, Yunfei Chu, Zeyu Cui, Kai Dang, Xiaodong Deng, Yang Fan, Wenbin Ge, Yu Han, Fei Huang, Binyuan Hui, Luo Ji, Mei Li, Junyang Lin, Runji Lin, Dayiheng Liu, Gao Liu, Chengqiang Lu, Keming Lu, and 29 others. 2023. [Qwen technical report](#). *Preprint*, arXiv:2309.16609.

Tom B. Brown, Benjamin Mann, Nick Ryder, Melanie Subbiah, Jared Kaplan, Prafulla Dhariwal, Arvind Neelakantan, Pranav Shyam, Girish Sastry, Amanda Askell, Sandhini Agarwal, Ariel Herbert-Voss, Gretchen Krueger, Tom Henighan, Rewon Child, Aditya Ramesh, Daniel M. Ziegler, Jeffrey Wu, Clemens Winter, and 12 others. 2020. [Language models are few-shot learners](#). *Preprint*, arXiv:2005.14165.

Yupeng Chang, Xu Wang, Jindong Wang, Yuan Wu, Linyi Yang, Kaijie Zhu, Hao Chen, Xiaoyuan Yi, Cunxiang Wang, Yidong Wang, and 1 others. 2024. A survey on evaluation of large language models. *ACM transactions on intelligent systems and technology*, 15(3):1–45.

Hardy Chen, Haoqin Tu, Fali Wang, Hui Liu, Xianfeng Tang, Xinya Du, Yuyin Zhou, and Cihang Xie. 2025a. [Sft or r1? an early investigation into training r1-like reasoning large vision-language models](#). *Preprint*, arXiv:2504.11468.

Junying Chen, Ruyi Ouyang, Anningzhe Gao, Shunian Chen, Guiming Hardy Chen, Xidong Wang, Ruifei Zhang, Zhenyang Cai, Ke Ji, Guangjun Yu, Xiang Wan, and Benyou Wang. 2024a. [Huatuogpt-vision, towards injecting medical visual knowledge into multimodal llms at scale](#). *Preprint*, arXiv:2406.19280.

Keqin Chen, Zhao Zhang, Weili Zeng, Richong Zhang, Feng Zhu, and Rui Zhao. 2023. [Shikra: Unleashing multimodal llm’s referential dialogue magic](#). *arXiv preprint arXiv:2306.15195*.

Lin Chen, Jinsong Li, Xiaoyi Dong, Pan Zhang, Conghui He, Jiaqi Wang, Feng Zhao, and Dahua Lin. 2024b. [Sharegpt4v: Improving large multi-modal models with better captions](#). In *European Conference on Computer Vision*, pages 370–387. Springer.

Weize Chen, Yusheng Su, Jingwei Zuo, Cheng Yang, Chenfei Yuan, Chi-Min Chan, Heyang Yu, Yaxi Lu, Yi-Hsin Hung, Chen Qian, and 1 others. 2024c. [Agentverse: Facilitating multi-agent collaboration and exploring emergent behaviors](#). In *ICLR*.

Yang Chen, Zhuolin Yang, Zihan Liu, Chankyu Lee, Peng Xu, Mohammad Shoeybi, Bryan Catanzaro, and Wei Ping. 2025b. [Acereason-nemotron: Advancing math and code reasoning through reinforcement learning](#). *arXiv preprint arXiv:2505.16400*.

Zhe Chen, Weiyun Wang, Yue Cao, Yangzhou Liu, Zhangwei Gao, Erfei Cui, Jinguo Zhu, Shenglong Ye, Hao Tian, Zhaoyang Liu, Lixin Gu, Xuehui Wang, Qingyun Li, Yiming Ren, Zixuan Chen, Jiapeng Luo, Jiahao Wang, Tan Jiang, Bo Wang, and 23 others. 2025c. [Expanding performance boundaries of open-source multimodal models with model, data, and test-time scaling](#). *Preprint*, arXiv:2412.05271.

XTuner Contributors. 2023. [Xtuner: A toolkit for efficiently fine-tuning llm](#). <https://github.com/InternLM/xtuner>.

DeepSeek-AI, Daya Guo, Dejian Yang, Haowei Zhang, Junxiao Song, Ruoyu Zhang, Runxin Xu, Qihao Zhu, Shirong Ma, Peiyi Wang, Xiao Bi, Xiaokang Zhang, Xingkai Yu, Yu Wu, Z. F. Wu, Zhibin Gou, Zhi-hong Shao, Zhuoshu Li, Ziyi Gao, and 181 others. 2025. *Deepseek-r1: Incentivizing reasoning capability in llms via reinforcement learning*. *Preprint*, arXiv:2501.12948.

Yuhao Dong, Zuyan Liu, Hai-Long Sun, Jingkang Yang, Winston Hu, Yongming Rao, and Ziwei Liu. 2025. Insight-v: Exploring long-chain visual reasoning with multimodal large language models. In *Proceedings of the Computer Vision and Pattern Recognition Conference*, pages 9062–9072.

Kaixuan Fan, Kaituo Feng, Haoming Lyu, Dongzhan Zhou, and Xiangyu Yue. 2025. *Sophiavl-r1: Reinforcing mllms reasoning with thinking reward*. *Preprint*, arXiv:2505.17018.

Yunhao Gou, Kai Chen, Zhili Liu, Lanqing Hong, Xin Jin, Zhenguo Li, James T. Kwok, and Yu Zhang. 2025a. Perceptual decoupling for scalable multi-modal reasoning via reward-optimized captioning. *arXiv preprint arXiv:2506.04559*.

Yunhao Gou, Kai Chen, Zhili Liu, Lanqing Hong, Xin Jin, Zhenguo Li, James T. Kwok, and Yu Zhang. 2025b. *Reasoning-aligned perception decoupling for scalable multi-modal reasoning*. *Preprint*, arXiv:2506.04559.

Lujun Gui and Qingnan Ren. 2025. Training reasoning model with dynamic advantage estimation on reinforcement learning. <https://www.notion.so/Training-Reasoning-Model-with-Dynamic-Advantage-Estimation-on-Reinforcement-Learning-1a830cc0904681fa9df3e076b6557a3e>. Notion Blog.

Tanmay Gupta and Aniruddha Kembhavi. 2023. Visual programming: Compositional visual reasoning without training. In *Proceedings of the IEEE/CVF conference on computer vision and pattern recognition*, pages 14953–14962.

Feng Han, Yang Jiao, Shaoxiang Chen, Junhao Xu, Jingjing Chen, and Yu-Gang Jiang. 2025a. Controlthinker: Unveiling latent semantics for controllable image generation through visual reasoning. *arXiv preprint arXiv:2506.03596*.

Junlin Han, Shengbang Tong, David Fan, Yufan Ren, Koustuv Sinha, Philip Torr, and Filippos Kokkinos. 2025b. *Learning to see before seeing: Demystifying llm visual priors from language pre-training*. *Preprint*, arXiv:2509.26625.

Xuehai He, Yichen Zhang, Luntian Mou, Eric Xing, and Pengtao Xie. 2020. Pathvqa: 30000+ questions for medical visual question answering. *arXiv preprint arXiv:2003.10286*.

Qidong Huang, Xiaoyi Dong, Pan Zhang, Bin Wang, Conghui He, Jiaqi Wang, Dahua Lin, Weiming Zhang, and Nenghai Yu. 2024. Opera: Alleviating hallucination in multi-modal large language models via over-trust penalty and retrospection-allocation. In *Proceedings of the IEEE/CVF Conference on Computer Vision and Pattern Recognition*, pages 13418–13427.

Wenxuan Huang, Bohan Jia, Zijie Zhai, Shaosheng Cao, Zheyu Ye, Fei Zhao, Zhe Xu, Yao Hu, and Shaohui Lin. 2025a. *Vision-r1: Incentivizing reasoning capability in multimodal large language models*. *Preprint*, arXiv:2503.06749.

Xiaoke Huang, Juncheng Wu, Hui Liu, Xianfeng Tang, and Yuyin Zhou. 2025b. Medvlthinker: Simple baselines for multimodal medical reasoning. *arXiv preprint*.

Yuxiang Ji, Ziyu Ma, Yong Wang, Guanhua Chen, Xiangxiang Chu, and Liaoni Wu. 2025. Tree search for llm agent reinforcement learning. *arXiv preprint arXiv:2509.21240*.

Songtao Jiang, Yuan Wang, Ruizhe Chen, Yan Zhang, Ruilin Luo, Bohan Lei, Sibo Song, Yang Feng, Jimeng Sun, Jian Wu, and Zuozhu Liu. 2025. Capo: Reinforcing consistent reasoning in medical decision-making. *Preprint*, arXiv:2506.12849.

Yubin Kim, Chanwoo Park, Hyewon Jeong, Yik Siu Chan, Xuhai Xu, Daniel McDuff, Hyeonhoon Lee, Marzyeh Ghassemi, Cynthia Breazeal, and Hae Won Park. 2024. *Magents: An adaptive collaboration of llms for medical decision-making*. *Preprint*, arXiv:2404.15155.

Takeshi Kojima, Shixiang Shane Gu, Machel Reid, Yutaka Matsuo, and Yusuke Iwasawa. 2022. Large language models are zero-shot reasoners. *Advances in neural information processing systems*, 35:22199–22213.

Keyi Kong, Xilie Xu, Di Wang, Jingfeng Zhang, and Mohan Kankanhalli. 2024. *Perplexity-aware correction for robust alignment with noisy preferences*. In *The Thirty-eighth Annual Conference on Neural Information Processing Systems*.

Woosuk Kwon, Zhuohan Li, Siyuan Zhuang, Ying Sheng, Lianmin Zheng, Cody Hao Yu, Joseph E. Gonzalez, Hao Zhang, and Ion Stoica. 2023. Efficient memory management for large language model serving with pagedattention. In *Proceedings of the ACM SIGOPS 29th Symposium on Operating Systems Principles*.

Jason J Lau, Soumya Gayen, Asma Ben Abacha, and Dina Demner-Fushman. 2018. A dataset of clinically generated visual questions and answers about radiology images. *Scientific data*, 5(1):1–10.

Sicong Leng, Hang Zhang, Guanzheng Chen, Xin Li, Shijian Lu, Chunyan Miao, and Lidong Bing. 2024. Mitigating object hallucinations in large vision-language models through visual contrastive decoding. In *Proceedings of the IEEE/CVF Conference*

*on Computer Vision and Pattern Recognition*, pages 13872–13882.

Ang Li, Charles Wang, Deqing Fu, Kaiyu Yue, Zikui Cai, Wang Bill Zhu, Ollie Liu, Peng Guo, Willie Neiswanger, Furong Huang, and 1 others. 2025a. Zebra-cot: A dataset for interleaved vision language reasoning. *arXiv preprint arXiv:2507.16746*.

Bo Li, Yuanhan Zhang, Dong Guo, Renrui Zhang, Feng Li, Hao Zhang, Kaichen Zhang, Peiyuan Zhang, Yanwei Li, Ziwei Liu, and Chunyuan Li. 2024. **Llava-onevision: Easy visual task transfer**. *Preprint*, arXiv:2408.03326.

Chunyuan Li, Cliff Wong, Sheng Zhang, Naoto Usuyama, Haotian Liu, Jianwei Yang, Tristan Naumann, Hoifung Poon, and Jianfeng Gao. 2023. Llava-med: Training a large language-and-vision assistant for biomedicine in one day. *arXiv preprint arXiv:2306.00890*.

Yuting Li, Lai Wei, Kaipeng Zheng, Jingyuan Huang, Guilin Li, Bo Wang, Linghe Kong, Lichao Sun, and Weiran Huang. 2025b. **Revisiting visual understanding in multimodal reasoning through a lens of image perturbation**. *Preprint*, arXiv:2506.09736.

Yiqing Liang, Jielin Qiu, Wenhao Ding, Zuxin Liu, James Tompkin, Mengdi Xu, Mengzhou Xia, Zhengzhong Tu, Laixi Shi, and Jiacheng Zhu. 2025. **Modomodo: Multi-domain data mixtures for multimodal llm reinforcement learning**. *Preprint*, arXiv:2505.24871.

Mengqi Liao, Xiangyu Xi, Ruinian Chen, Jia Leng, Yagen Hu, Ke Zeng, Shuai Liu, and Huaiyu Wan. 2025. **Enhancing efficiency and exploration in reinforcement learning for llms**. *Preprint*, arXiv:2505.18573.

Kevin Qinghong Lin, Yuhao Zheng, Hangyu Ran, Dantong Zhu, Dongxing Mao, Linjie Li, Philip Torr, and Alex Jinpeng Wang. 2025. **Vcode: a multimodal coding benchmark with svg as symbolic visual representation**. *Preprint*, arXiv:2511.02778.

Bo Liu, Li-Ming Zhan, Li Xu, Lin Ma, Yan Yang, and Xiao-Ming Wu. 2021. **Slake: A semantically-labeled knowledge-enhanced dataset for medical visual question answering**. *Preprint*, arXiv:2102.09542.

Haogeng Liu, Quanzeng You, Xiaotian Han, Yongfei Liu, Huabo Huang, Ran He, and Hongxia Yang. 2024a. Visual anchors are strong information aggregators for multimodal large language model. *arXiv preprint arXiv:2405.17815*.

Haotian Liu, Chunyuan Li, Yuheng Li, Bo Li, Yuanhan Zhang, Sheng Shen, and Yong Jae Lee. 2024b. **Llava-next: Improved reasoning, ocr, and world knowledge**.

Shilong Liu, Hao Cheng, Haotian Liu, Hao Zhang, Feng Li, Tianhe Ren, Xueyan Zou, Jianwei Yang, Hang Su, Jun Zhu, Lei Zhang, Jianfeng Gao, and Chunyuan Li. 2023. **Llava-plus: Learning to use tools for creating multimodal agents**. *Preprint*, arXiv:2311.05437.

Xiangyan Liu, Jinjie Ni, Zijian Wu, Chao Du, Longxu Dou, Haonan Wang, Tianyu Pang, and Michael Qizhe Shieh. 2025a. **Noisyrollout: Reinforcing visual reasoning with data augmentation**. *arXiv preprint arXiv:2504.13055*.

Ziyu Liu, Yuhang Zang, Yushan Zou, Zijian Liang, Xiaoyi Dong, Yuhang Cao, Haodong Duan, Dahua Lin, and Jiaqi Wang. 2025b. **Visual agentic reinforcement fine-tuning**. *Preprint*, arXiv:2505.14246.

Zongkai Liu, Fanqing Meng, Lingxiao Du, Zhixiang Zhou, Chao Yu, Wenqi Shao, and Qiaosheng Zhang. 2025c. **Cpgd: Toward stable rule-based reinforcement learning for language models**. *Preprint*, arXiv:2505.12504.

Pan Lu, Hritik Bansal, Tony Xia, Jiacheng Liu, Chunyuan Li, Hannaneh Hajishirzi, Hao Cheng, Kai-Wei Chang, Michel Galley, and Jianfeng Gao. 2024. Mathvista: Evaluating mathematical reasoning of foundation models in visual contexts. In *International Conference on Learning Representations (ICLR)*.

Pan Lu, Ran Gong, Shibiao Jiang, Liang Qiu, Siyuan Huang, Xiaodan Liang, and Song-Chun Zhu. 2021. **Inter-gps: Interpretable geometry problem solving with formal language and symbolic reasoning**. In *The Joint Conference of the 59th Annual Meeting of the Association for Computational Linguistics and the 11th International Joint Conference on Natural Language Processing (ACL-IJCNLP 2021)*.

Pan Lu, Baolin Peng, Hao Cheng, Michel Galley, Kai-Wei Chang, Ying Nian Wu, Song-Chun Zhu, and Jianfeng Gao. 2023. **Chameleon: Plug-and-play compositional reasoning with large language models**. *Advances in Neural Information Processing Systems*, 36:43447–43478.

Ruilin Luo, Zhuofan Zheng, Yifan Wang, Yiyao Yu, Xinze Ni, Zicheng Lin, Jin Zeng, and Yujiu Yang. 2025. **Ursa: Understanding and verifying chain-of-thought reasoning in multimodal mathematics**. *arXiv preprint arXiv:2501.04686*.

Yunze Man, De-An Huang, Guilin Liu, Shiwei Sheng, Shilong Liu, Liang-Yan Gui, Jan Kautz, Yu-Xiong Wang, and Zhiding Yu. 2025. **Argus: Vision-centric reasoning with grounded chain-of-thought**. In *Proceedings of the Computer Vision and Pattern Recognition Conference*, pages 14268–14280.

Fanqing Meng, Lingxiao Du, Zongkai Liu, Zhixiang Zhou, Quanfeng Lu, Daocheng Fu, Tiancheng Han, Botian Shi, Wenhui Wang, Junjun He, Kaipeng Zhang, Ping Luo, Yu Qiao, Qiaosheng Zhang, and Wenqi Shao. 2025a. **Mm-eureka: Exploring the frontiers of multimodal reasoning with rule-based reinforcement learning**. *Preprint*, arXiv:2503.07365.

Fanqing Meng, Lingxiao Du, Zongkai Liu, Zhixiang Zhou, Quanfeng Lu, Daocheng Fu, Botian Shi, Wenhui Wang, Junjun He, Kaipeng Zhang, and 1 others. 2025b. **Mm-eureka: Exploring visual aha moment**

with rule-based large-scale reinforcement learning. *arXiv preprint arXiv:2503.07365*.

Michael Moor, Qian Huang, Shirley Wu, Michihiro Yasunaga, Cyril Zakka, Yash Dalmia, Eduardo Pontes Reis, Pranav Rajpurkar, and Jure Leskovec. 2023. **Med-flamingo: a multimodal medical few-shot learner**. *Preprint*, arXiv:2307.15189.

Long Ouyang, Jeff Wu, Xu Jiang, Diogo Almeida, Carroll L. Wainwright, Pamela Mishkin, Chong Zhang, Sandhini Agarwal, Katarina Slama, Alex Ray, John Schulman, Jacob Hilton, Fraser Kelton, Luke Miller, Maddie Simens, Amanda Askell, Peter Welinder, Paul Christiano, Jan Leike, and Ryan Lowe. 2022. **Training language models to follow instructions with human feedback**. *Preprint*, arXiv:2203.02155.

Prasanna Parthasarathi, Mathieu Reymond, Boxing Chen, Yufei Cui, and Sarath Chandar. 2025. **Grpo- $\lambda$ : Credit assignment improves llm reasoning**. *Preprint*, arXiv:2510.00194.

Adam Paszke, Sam Gross, Francisco Massa, Adam Lerer, James Bradbury, Gregory Chanan, Trevor Killeen, Zeming Lin, Natalia Gimelshein, Luca Antiga, Alban Desmaison, Andreas Köpf, Edward Yang, Zach DeVito, Martin Raison, Alykhan Tejani, Sasank Chilamkurthy, Benoit Steiner, Lu Fang, and 2 others. 2019. **Pytorch: An imperative style, high-performance deep learning library**. *Preprint*, arXiv:1912.01703.

Ji Qi, Ming Ding, Weihan Wang, Yushi Bai, Qingsong Lv, Wenyi Hong, Bin Xu, Lei Hou, Juanzi Li, Yuxiao Dong, and 1 others. 2024. **Cogcom: A visual language model with chain-of-manipulations reasoning**. *arXiv preprint arXiv:2402.04236*.

Runqi Qiao, Qiuna Tan, Guanting Dong, Minhui Wu, Chong Sun, Xiaoshuai Song, Zhuoma GongQue, Shanglin Lei, Zhe Wei, MiaoXuan Zhang, and 1 others. 2024. **We-math: Does your large multimodal model achieve human-like mathematical reasoning?** *arXiv preprint arXiv:2407.01284*.

Qwen, :, An Yang, Baosong Yang, Beichen Zhang, Binyuan Hui, Bo Zheng, Bowen Yu, Chengyuan Li, Dayiheng Liu, Fei Huang, Haoran Wei, Huan Lin, Jian Yang, Jianhong Tu, Jianwei Zhang, Jianxin Yang, Jiaxi Yang, Jingren Zhou, and 25 others. 2025. **Qwen2.5 technical report**. *Preprint*, arXiv:2412.15115.

Gabriel Sarch, Snigdha Saha, Naitik Khandelwal, Ayush Jain, Michael J Tarr, Aviral Kumar, and Katerina Fragkiadaki. 2025. **Grounded reinforcement learning for visual reasoning**. *arXiv preprint arXiv:2505.23678*.

Zhihong Shao, Peiyi Wang, Qihao Zhu, Runxin Xu, Junxiao Song, Xiao Bi, Haowei Zhang, Mingchuan Zhang, Y. K. Li, Y. Wu, and Daya Guo. 2024. **Deepseekmath: Pushing the limits of mathematical reasoning in open language models**. *Preprint*, arXiv:2402.03300.

Yongliang Shen, Kaitao Song, Xu Tan, Dongsheng Li, Weiming Lu, and Yueting Zhuang. 2023. **Hugging-gpt: Solving ai tasks with chatgpt and its friends in hugging face**. *Advances in Neural Information Processing Systems*, 36:38154–38180.

Zhaochen Su, Peng Xia, Hangyu Guo, Zhenhua Liu, Yan Ma, Xiaoye Qu, Jiaqi Liu, Yanshu Li, Kaide Zeng, Zhengyuan Yang, and 1 others. 2025. **Thinking with images for multimodal reasoning: Foundations, methods, and future frontiers**. *arXiv preprint arXiv:2506.23918*.

Haoran Sun, Yankai Jiang, Wenjie Lou, Yujie Zhang, Wenjie Li, Lilong Wang, Mianxin Liu, Lei Liu, and Xiaosong Wang. 2023. **Chiron-o1: Igniting multimodal large language models towards generalizable medical reasoning via mentor-intern collaborative search**. In *The Thirty-ninth Annual Conference on Neural Information Processing Systems*.

Dídac Surís, Sachit Menon, and Carl Vondrick. 2023. **Vipergpt: Visual inference via python execution for reasoning**. In *Proceedings of the IEEE/CVF international conference on computer vision*, pages 11888–11898.

Xiangru Tang, Anni Zou, Zhuosheng Zhang, Ziming Li, Yilun Zhao, Xingyao Zhang, Arman Cohan, and Mark Gerstein. 2024. **Medagents: Large language models as collaborators for zero-shot medical reasoning**. In *Findings of the Association for Computational Linguistics: ACL 2024*, pages 599–621.

Haozhe Wang, Chao Qu, Zuming Huang, Wei Chu, Fangzhen Lin, and Wenhui Chen. 2025a. **VI-rethinker: Incentivizing self-reflection of vision-language models with reinforcement learning**. *arXiv preprint arXiv:2504.08837*.

Jiacong Wang, Zijian Kang, Haochen Wang, Haiyong Jiang, Jiawen Li, Bohong Wu, Ya Wang, Jiao Ran, Xiao Liang, Chao Feng, and 1 others. 2025b. **Vgr: Visual grounded reasoning**. *arXiv preprint arXiv:2506.11991*.

Jiaqi Wang, Hanqi Jiang, Yiheng Liu, Chong Ma, Xu Zhang, Yi Pan, Mengyuan Liu, Peiran Gu, Sichen Xia, Wenjun Li, and 1 others. 2024a. **A comprehensive review of multimodal large language models: Performance and challenges across different tasks**. *arXiv preprint arXiv:2408.01319*.

Peng Wang, Shuai Bai, Sinan Tan, Shijie Wang, Zhihao Fan, Jinze Bai, Keqin Chen, Xuejing Liu, Jialin Wang, Wenbin Ge, Yang Fan, Kai Dang, Mengfei Du, Xuancheng Ren, Rui Men, Dayiheng Liu, Chang Zhou, Jingren Zhou, and Junyang Lin. 2024b. **Qwen2-vl: Enhancing vision-language model’s perception of the world at any resolution**. *Preprint*, arXiv:2409.12191.

Xiayao Wang, Chunyuan Li, Jianwei Yang, Kai Zhang, Bo Liu, Tianyi Xiong, and Furong Huang. 2025c. **Llava-critic-r1: Your critic model is secretly a strong policy model**. *Preprint*, arXiv:2509.00676.

Xiyao Wang, Zhengyuan Yang, Chao Feng, Hongjin Lu, Linjie Li, Chung-Ching Lin, Kevin Lin, Furong Huang, and Lijuan Wang. 2025d. Sota with less: Mcts-guided sample selection for data-efficient visual reasoning self-improvement. *arXiv preprint arXiv:2504.07934*.

Yiping Wang, Qing Yang, Zhiyuan Zeng, Liliang Ren, Liyuan Liu, Baolin Peng, Hao Cheng, Xuehai He, Kuan Wang, Jianfeng Gao, Weizhu Chen, Shuohang Wang, Simon Shaolei Du, and Yelong Shen. 2025e. Reinforcement learning for reasoning in large language models with one training example. *Preprint*, arXiv:2504.20571.

Yuan Wang, Shujian Gao, Jiaxiang Liu, Songtao Jiang, Haoxiang Xia, Xiaotian Zhang, Zhaolu Kang, Yemin Wang, and Zuozhu Liu. 2025f. Beyond n-grams: A hierarchical reward learning framework for clinically-aware medical report generation. *arXiv preprint arXiv:2512.02710*.

Zhenhailong Wang, Xuehang Guo, Sofia Stoica, Haiyang Xu, Hongru Wang, Hyeonjeong Ha, Xiusi Chen, Yangyi Chen, Ming Yan, Fei Huang, and Heng Ji. 2025g. Perception-aware policy optimization for multimodal reasoning. *Preprint*, arXiv:2507.06448.

Chaoyi Wu, Xiaoman Zhang, Ya Zhang, Yanfeng Wang, and Weidi Xie. 2023. Towards generalist foundation model for radiology by leveraging web-scale 2d&3d medical data. *Preprint*, arXiv:2308.02463.

Mingyuan Wu, Jingcheng Yang, Jize Jiang, Meitang Li, Kaizhuo Yan, Hanchao Yu, Minjia Zhang, Chengxiang Zhai, and Klara Nahrstedt. 2025. Vtool-r1: Vlms learn to think with images via reinforcement learning on multimodal tool use. *arXiv preprint arXiv:2505.19255*.

Peng Xia, Jinglu Wang, Yibo Peng, Kaide Zeng, Xian Wu, Xiangru Tang, Hongtu Zhu, Yun Li, Shujie Liu, Yan Lu, and Huaxiu Yao. 2025. Mmedagent-rl: Optimizing multi-agent collaboration for multimodal medical reasoning. *Preprint*, arXiv:2506.00555.

Yi Yang, Xiaoxuan He, Hongkun Pan, Xiyuan Jiang, Yan Deng, Xingtao Yang, Haoyu Lu, Dacheng Yin, Fengyun Rao, Minfeng Zhu, Bo Zhang, and Wei Chen. 2025. R1-onevision: Advancing generalized multimodal reasoning through cross-modal formalization. *arXiv preprint arXiv:2503.10615*.

Yixin Ye, Zhen Huang, Yang Xiao, Ethan Chern, Shijie Xia, and Pengfei Liu. 2025. Limo: Less is more for reasoning. *arXiv preprint arXiv:2502.03387*.

Qiyi Yu, Zheng Zhang, Ruofei Zhu, Yufeng Yuan, Xiaochen Zuo, Yu Yue, Weinan Dai, Tiantian Fan, Gaohong Liu, Lingjun Liu, Xin Liu, Haibin Lin, Zhiqi Lin, Bole Ma, Guangming Sheng, Yuxuan Tong, Chi Zhang, Mofan Zhang, Wang Zhang, and 16 others. 2025. Dapo: An open-source llm reinforcement learning system at scale. *Preprint*, arXiv:2503.14476.

Xiang Yue, Yuansheng Ni, Kai Zhang, Tianyu Zheng, Ruoqi Liu, Ge Zhang, Samuel Stevens, Dongfu Jiang, Weiming Ren, Yuxuan Sun, Cong Wei, Botao Yu, Ruibin Yuan, Renliang Sun, Ming Yin, Boyuan Zheng, Zhenzhu Yang, Yibo Liu, Wenhao Huang, and 3 others. 2024a. Mmmu: A massive multi-discipline multimodal understanding and reasoning benchmark for expert agi. In *Proceedings of CVPR*.

Xiang Yue, Yuansheng Ni, Kai Zhang, Tianyu Zheng, Ruoqi Liu, Ge Zhang, Samuel Stevens, Dongfu Jiang, Weiming Ren, Yuxuan Sun, and 1 others. 2024b. Mmmu: A massive multi-discipline multimodal understanding and reasoning benchmark for expert agi. In *Proceedings of the IEEE/CVF Conference on Computer Vision and Pattern Recognition*, pages 9556–9567.

Haoji Zhang, Xin Gu, Jiawen Li, Chixiang Ma, Sule Bai, Chubin Zhang, Bowen Zhang, Zhichao Zhou, Dongliang He, and Yansong Tang. 2025a. Thinking with videos: Multimodal tool-augmented reinforcement learning for long video reasoning. *arXiv preprint arXiv:2508.04416*.

Jiayi Zhang, Jinyu Xiang, Zhaoyang Yu, Fengwei Teng, Xionghui Chen, Jiaqi Chen, Mingchen Zhuge, Xin Cheng, Sirui Hong, Jinlin Wang, Bingnan Zheng, Bang Liu, Yuyu Luo, and Chenglin Wu. 2025b. Aflow: Automating agentic workflow generation. *Preprint*, arXiv:2410.10762.

Jingyi Zhang, Jiaxing Huang, Huanjin Yao, Shunyu Liu, Xikun Zhang, Shijian Lu, and Dacheng Tao. 2025c. R1-vl: Learning to reason with multimodal large language models via step-wise group relative policy optimization. *arXiv preprint arXiv:2503.12937*.

Jixiao Zhang and Chunsheng Zuo. 2025. Grpo-lead: A difficulty-aware reinforcement learning approach for concise mathematical reasoning in language models. *Preprint*, arXiv:2504.09696.

Renrui Zhang, Dongzhi Jiang, Yichi Zhang, Haokun Lin, Ziyu Guo, Pengshuo Qiu, Aojun Zhou, Pan Lu, Kai-Wei Chang, Peng Gao, and Hongsheng Li. 2024a. Mathverse: Does your multi-modal llm truly see the diagrams in visual math problems? *Preprint*, arXiv:2403.14624.

Xiaoman Zhang, Chaoyi Wu, Ziheng Zhao, Weixiong Lin, Ya Zhang, Yanfeng Wang, and Weidi Xie. 2024b. Pmc-vqa: Visual instruction tuning for medical visual question answering. *Preprint*, arXiv:2305.10415.

Yuting Zhang, Kaishen Yuan, Hao Lu, Yutao Yue, Jintai Chen, and Kaishun Wu. 2025d. Medvt-r1: A multimodal llm empowering medical reasoning and diagnosis. *Preprint*, arXiv:2506.18512.

Zhuosheng Zhang, Aston Zhang, Mu Li, Hai Zhao, George Karypis, and Alex Smola. 2024c. Multimodal chain-of-thought reasoning in language models. *Preprint*, arXiv:2302.00923.

Yaowei Zheng, Junting Lu, Shenzhi Wang, Zhangchi Feng, Dongdong Kuang, and Yuwen Xiong. 2025a. Easyr1: An efficient, scalable, multi-modality rl training framework.

Ziwei Zheng, Michael Yang, Jack Hong, Chenxiao Zhao, Guohai Xu, Le Yang, Chao Shen, and Xing Yu. 2025b. Deepeyes: Incentivizing" thinking with images" via reinforcement learning. *arXiv preprint arXiv:2505.14362*.

Yuxin Zuo, Shang Qu, Yifei Li, Zhangren Chen, Xuekai Zhu, Ermo Hua, Kaiyan Zhang, Ning Ding, and Bowen Zhou. 2025. Medxpertqa: Benchmarking expert-level medical reasoning and understanding. *Preprint*, arXiv:2501.18362.

## A Appendix

This appendix provides implementation details, additional quantitative ablations, and extensive qualitative examples to support the findings in the main paper. The organization is as follows:

- **§B Implementation Details.** We provide a detailed breakdown of our experimental setup, including:

- **§B.1 Evaluation Details:** Detailed protocols for Mathematical and Medical benchmarks.
- **§B.2 Hyperparameter:** Comprehensive lists of training hyperparameters and DVPD coefficients.
- **§B.3 Prompt Template:** The standardized system prompt and reasoning template used across all experiments.
- **§B.4 Noise Scheduling:** We detail the variance-preserving diffusion formulation and the Sigmoid annealing schedule employed to dynamically modulate noise intensity, implementing a curriculum learning strategy for visual robustness.

- **§C Ablation on Perturbation Parameters.** We present the sensitivity analysis for masking ratios ( $P_{mask}$ ) and noise steps ( $T_{init}$ ).

- **§D Visual Robustness and Sensitivity Analysis.** We analyze the contrasting behaviors of MLLMs under diffusion noise versus semantic masking.

- **§E RL Visual Dependency Experiments.** We detail the blind experiments (Text-Only and Blank Image) used to verify visual grounding.

- **§F Qualitative Analysis of Visual Dependency.** We provide case studies demonstrating linguistic shortcuts in baseline methods under blind settings.
- **§G Qualitative Comparison of RLVR Algorithms.** We offer a comparative visualization of reasoning trajectories between GRPO, DAPO, and our DVPD.

## B Implementation Details

### B.1 Evaluation Details

**Evaluation Protocols.** To comprehensively assess model performance, we conducted evaluations across both general (mathematical) and medical domains, distinguishing between in-domain and out-of-domain (OOD) settings.

- **Mathematical Evaluation:** We employed Geo3k (Lu et al., 2021), Vista (Lu et al., 2024), WeMath (Qiao et al., 2024), MVerse (Zhang et al., 2024a), MVerse-V (Zhang et al., 2024a), and MMKI2 (Meng et al., 2025b) as OOD benchmarks to test generalization capabilities. Furthermore, we utilized mathruler.grader to facilitate precise evaluation.
- **Medical Evaluation:** We utilized the test splits of Slake (Liu et al., 2021), PathVQA (He et al., 2020), RadVQA (Lau et al., 2018), and PMC-VQA (Zhang et al., 2024b) for in-domain evaluation. Furthermore, MedXpertQA (Zuo et al., 2025) and MMMU-Med (Yue et al., 2024a) were employed to assess OOD performance.

To ensure the statistical reliability of our results, we report the Average Accuracy over 8 runs (**AVG@8 Acc**). For inference, we deployed the vLLM engine to accelerate generation (Kwon et al., 2023). For fair comparison, all models utilized a unified system prompt (reasoning template) to elicit chain-of-thought reasoning, with the temperature set to 1.0 and top-p to 0.9. The specific templates used are detailed in Appendix B.3.

**Baselines.** To conduct a comprehensive comparative analysis, we evaluate our proposed method against baselines categorized into two distinct dimensions: RL-based optimization methods and foundational MLLMs.

*RL-based Methods.* We benchmark our approach against state-of-the-art RL strategies de-

signed for reasoning or visual alignment, including **GRPO** (Shao et al., 2024), **DAPO** (Yu et al., 2025), **PAPO** (Wang et al., 2025g), and **NoiseRoll-out** (Liu et al., 2025a). To ensure a fair comparison, we re-trained these RL methods using the identical training set and evaluation suite.

*Foundation Models.* We compare against a diverse spectrum of baselines ranging from proprietary commercial systems to specialized open-source models:

- *Medical-Specific Models:* We evaluate performant open-source models tailored for the biomedical domain, such as **HuatuoGPT-Vision-34B** (Chen et al., 2024a).
- *Math-Specific Models:* For mathematical reasoning tasks, we include domain-expert models like **MM-Eureka** (Meng et al., 2025a) and **ThinkLite-7B** (Wang et al., 2025d).
- *General-Purpose Models:* We also include widely adopted general open-source benchmarks, such as **Qwen-VL** (Bai et al., 2023) and **LLaVA-v1.6** (Liu et al., 2024b).

## B.2 Hyperparameter

To ensure reproducibility, we provide a comprehensive overview of the training and evaluation hyperparameters in Table 5 and Table 6. All models are optimized using AdamW with a constant learning rate of 1e-6 and a global batch size of 128. Consistent with recent reinforcement learning practices, we remove the KL penalty relative to the reference model to facilitate broader policy exploration (Liu et al., 2025a; Yu et al., 2025).

Crucially, our **DVRP** framework introduces three auxiliary objectives regulated by specific coefficients: Visual Robustness ( $\lambda_{rob} = 0.01$ ), Visual Sensitivity ( $\lambda_{nec} = 0.01$ ), and Entropy Regularization ( $\lambda_{ent} = 0.05$ ). The above loss weights are consistent with previous works (Wang et al., 2025g; Liu et al., 2025a). To address the varying information density of visual modalities, we employ domain-adaptive perturbation strategies. As detailed in Table 5, we apply a higher mask probability ( $P_{mask} = 0.6$ ) and longer noise injection steps ( $T_{init} = 500$ ) for mathematical reasoning, while adopting milder perturbations ( $P_{mask} = 0.2, T_{init} = 100$ ) for medical tasks to preserve fine-grained pathological details.

Hyperparameter	Value
<i>General Training</i>	
Optimizer	AdamW (BF16)
Learning Rate	1e-6
LR Schedule	Constant
Total Epochs	3
<i>RL Process (GRPO)</i>	
Global Batch Size	128
Rollout Batch Size	384
Group Size ( $G$ )	5
KL Penalty (Ref Model)	None (Disabled)
Reward Signal	Accuracy
<i>DVRP Objectives</i>	
Visual Robustness Loss ( $\lambda_{rob}$ )	0.01
Visual Sensitivity Loss ( $\lambda_{nec}$ )	0.01
Entropy Regularization ( $\lambda_{ent}$ )	0.05
<i>Visual Perturbation</i>	
Mask Probability ( $P_{mask}$ )	0.6 / 0.2
Patch Size ( $P_{mask}$ )	14 / 14
Noise Steps ( $T_{init}$ )	500 / 100
<i>Inference</i>	
Temperature	1.0
Top-p	0.99
Max New Tokens	2048
<i>Resources &amp; Efficiency</i>	
Compute	4× NVIDIA A800
Step Time	~1000–2000s

Table 5: Key hyperparameters for training and evaluation. DVRP parameters vary by domain (Math vs. Medical). Notations correspond to Eq. (4).

## B.3 Prompt Template

For the prompt selection, we employ a standardized template across all training and evaluation stages to elicit stable Chain-of-Thought (CoT) reasoning. As illustrated in Figure 3, the template explicitly instructs the model to generate an internal monologue within `<think>` tags before producing the final answer, ensuring the output format remains consistent for automated parsing and reward calculation.

## B.4 Noise Scheduling

We adopt a variance-preserving (VP) diffusion process to construct the incremental view  $I_{noise}$ , simulating environmental instability while maintaining semantic consistency. Given an original image  $I$  and a noise intensity coefficient  $\beta \in [0, 1]$ , the perturbed input is formulated as:

$$I_{noise} = \sqrt{1 - \beta} \cdot I + \sqrt{\beta} \cdot \epsilon, \quad \epsilon \sim \mathcal{N}(0, \mathbf{I}) \quad (5)$$

Hyperparameter	Value
<i>General Training</i>	
Optimizer	AdamW (BF16)
Learning Rate	1e-6
LR Schedule	Constant
Total Epochs	3
<i>RL Process (DAPO)</i>	
Global Batch Size	128
Rollout Batch Size	384
Mini-Rollout Batch Size	128
Group Size ( $G$ )	5
KL Penalty (Ref Model)	None (Disabled)
Reward Signal	Accuracy
<i>DVRP Objectives</i>	
Visual Robustness Loss ( $\lambda_{rob}$ )	0.01
Visual Sensitivity Loss ( $\lambda_{nec}$ )	0.01
Entropy Regularization ( $\lambda_{ent}$ )	0.05
<i>Visual Perturbation</i>	
Mask Probability ( $P_{mask}$ )	0.6 / 0.2
Patch Size ( $P_{mask}$ )	14 / 14
Noise Steps ( $T_{init}$ )	500 / 100
<i>Inference</i>	
Temperature	1.0
Top-p	0.99
Max New Tokens	2048
<i>Resources &amp; Efficiency</i>	
Compute	4× NVIDIA A800
Step Time	~1000–2000s

Table 6: Key hyperparameters for training and evaluation based on the DAPO + DVRP configuration.

where  $\epsilon$  represents standard Gaussian noise. The coefficient  $\beta$  determines the signal-to-noise ratio; a higher  $\beta$  introduces stronger perturbation.

To balance structural robustness learning with convergence stability, we introduce a curriculum learning strategy via a Sigmoid decay schedule. Specifically, the noise intensity  $\beta$  is dynamically annealed based on the training progress. Let  $k$  be the current training step and  $K$  be the total steps. We compute the diffusion timestep  $t$  as:

$$t(k) = T_{init} \cdot \sigma \left( \gamma \cdot \left( 0.5 - \frac{k}{K} \right) \right), \quad (6)$$

where  $T_{init}$  is the initial noise step (e.g., 500),  $\sigma(\cdot)$  is the sigmoid function, and  $\gamma$  is a scaling factor controlling the decay steepness (set to 10 in our experiments). The noise intensity is then derived as  $\beta_k = t(k)/T_{max}$ . This schedule imposes high-variance perturbations in the early stages to enforce broad structural invariance, while gradually annealing the noise to zero to refine fine-grained visual

consistency.

## C Ablation on Perturbation Parameters

We investigate the sensitivity of the DVRP framework to the intensity of visual perturbations. We perform ablations on the Qwen2.5-VL-7B (Qwen et al., 2025) backbone by varying the masking ratio  $P_{mask} \in \{0.2, 0.4, 0.6\}$  and the noise injection steps  $T_{init} \in \{100, 300, 500\}$ . The results are detailed in Table 7.

**Masking Ratio.** We observe a distinct divergence in optimal masking ratios between domains. For **General Multimodal Reasoning** (e.g., Math), performance improves consistently as the masking ratio increases, peaking at  $P_{mask} = 0.6$ . This suggests that geometric diagrams and natural images contain high spatial redundancy; aggressive masking effectively forces the model to learn structural dependencies rather than relying on local textures. In contrast, **Medical Multimodal Reasoning** favors a conservative ratio ( $P_{mask} = 0.2$ ). Performance drops significantly (from 74.3% to 71.4%) when the ratio is increased to 0.6. This indicates that medical diagnosis relies heavily on fine-grained visual details (e.g., small lesions or boundaries), which are easily destroyed by aggressive occlusion.

**Noise Injection Level.** A similar trend is observed for noise robustness. We implement noise injection via a diffusion process, utilizing a sigmoid schedule to modulate the noise intensity. In the general domain, the model benefits from stronger consistency regularization, achieving peak accuracy with higher diffusion timesteps ( $T_{init} = 500$ ). Conversely, the medical domain is sensitive to high-intensity diffusion perturbations. Performance degrades as  $T_{init}$  increases, with the optimal setting found at a lower timestep ( $T_{init} = 100$ ). We hypothesize that excessive diffusion noise in medical images risks corrupting subtle pathological features or mimicking sensor artifacts, thereby confusing the reasoning policy.

Based on these observations, our final  $\mathbf{DVRP}_G$  model adopts domain-specific settings: we apply stronger perturbations ( $P = 0.6, T = 500$ ) for math tasks to encourage robustness, and milder perturbations ( $P = 0.2, T = 100$ ) for medical tasks to preserve visual fidelity.

**Impact of Noise Structure.** Table 8 further scrutinizes the efficacy of structured *Diffusion Noise*

Method / Setting	General Multimodal Reasoning							Medical Multimodal Reasoning				Overall	
	Geo3k	Vista	WeMath	MVerse	MVerse-V	MMKI2	AVG	Slake	Path	Rad	PMC	AVG	AVG
<i>Qwen2.5-VL-7B Backbone</i>													
Base Model (Original)	33.8	55.9	41.8	45.6	36.9	43.7	43.0	63.7	60.6	61.3	52.2	59.5	49.6
Baseline (GRPO)	40.2	65.5	66.1	66.5	61.7	72.1	62.0	74.7	75.7	74.9	56.2	70.4	65.4
<b>Ablation I: Sensitivity to Masking Ratio (<math>P_{mask}</math>)</b> (Math favors high mask, Medical favors low mask)													
+ Masking ( $P = 0.2$ )	41.0	68.2	66.8	66.9	63.5	73.5	63.3	78.5	<b>79.2</b>	78.2	61.4	<b>74.3</b>	67.7
+ Masking ( $P = 0.4$ )	41.8	69.5	67.5	67.1	65.1	74.8	64.3	76.8	78.1	77.4	60.2	73.1	67.8
+ Masking ( $P = 0.6$ )	<b>42.3</b>	<b>71.1</b>	<b>68.1</b>	<b>67.4</b>	<b>66.7</b>	<b>75.6</b>	<b>65.2</b>	74.5	76.5	75.8	58.9	71.4	67.7
<b>Ablation II: Robustness to Noise Injection (<math>T_{init}</math>)</b> (Math needs strong noise, Medical needs weak noise)													
+ Noise ( $T = 100$ )	41.2	68.5	66.9	67.0	64.2	73.9	63.6	76.2	76.5	<b>80.2</b>	59.1	<b>73.0</b>	67.4
+ Noise ( $T = 300$ )	41.9	70.1	67.6	67.2	65.8	74.9	64.6	75.1	75.8	78.4	57.8	71.8	67.5
+ Noise ( $T = 500$ )	<b>42.3</b>	<b>71.1</b>	<b>68.1</b>	<b>67.4</b>	<b>66.7</b>	<b>75.6</b>	<b>65.2</b>	73.5	74.2	76.1	56.5	70.1	67.2
<b>DVRP<sub>G</sub> (Optimal)</b>	<b>42.3</b>	<b>71.1</b>	<b>68.1</b>	67.4	<b>66.7</b>	<b>75.6</b>	<b>65.2</b>	<b>81.7</b>	78.3	79.9	<b>65.5</b>	<b>76.4</b>	<b>69.7</b>

Table 7: Comprehensive ablation study of the DVRP framework on Qwen2.5-VL-7B. We systematically vary the **Masking Ratio** ( $P_{mask} \in \{0.2, 0.4, 0.6\}$ ) and **Noise Steps** ( $T_{init} \in \{100, 300, 500\}$ ). The results highlight a domain-specific dichotomy: **General/Math** tasks benefit from aggressive perturbations ( $P = 0.6, T = 500$ ) to enforce structural reasoning, whereas **Medical** tasks require milder regularization ( $P = 0.2, T = 100$ ) to preserve fine-grained pathological features. The final **DVRP<sub>G</sub>** model employs these domain-optimal settings.

Method / Setting	Medical Multimodal Reasoning				
	Slake	Path	Rad	PMC	AVG
Base Model (Original)	63.7	60.6	61.3	52.2	59.5
Baseline (GRPO)	74.7	75.7	74.9	56.2	70.4
<b>Comparison of Noise Types</b> (Fixed scheduling, varying structure)					
+ Gaussian Noise ( $\sigma = 0.1$ )	75.2	76.0	76.5	57.0	71.2
+ Diffusion Noise ( $T = 100$ )	<b>76.2</b>	<b>76.5</b>	<b>80.2</b>	<b>59.1</b>	<b>73.0</b>

Table 8: Ablation study comparing noise injection strategies in the Medical domain. Under the DVRP framework, structured **Diffusion Noise** ( $T = 100$ ) outperforms unstructured **Gaussian Noise** ( $\sigma = 0.1$ ) by **+1.8%**, demonstrating that preserving semantic structure during perturbation is critical for medical visual reasoning.

( $T = 100$ ) versus unstructured **Gaussian Noise** ( $\sigma = 0.1$ ) in the medical domain ( $P = 0.6$ ). The results demonstrate that Diffusion Noise consistently outperforms Gaussian Noise, achieving an average gain of **+1.8%**. This suggests that structured perturbations effectively regularize the policy while preserving essential semantic integrity, whereas unstructured Gaussian noise risks degrading the pixel-level fidelity required for fine-grained medical diagnostics.

## D Visual Robustness and Sensitivity Analysis

To investigate the reliance of MLLMs on visual fidelity and their resilience to perturbations, we conduct a comprehensive robustness analysis on Qwen2.5-VL benchmarks (Qwen et al., 2025) across general and medical domains. We introduce

two distinct types of visual perturbations: Diffusion Noise, which represents high-frequency corruption, and Patch Masking, which represents semantic information loss. As visualized in Figure 4, these perturbations induce contrasting reasoning behaviors: the model remains resilient and consistent under noise ( $+\Delta$ ) but becomes confused and divergent when visual semantics are masked ( $-\Delta$ ). This qualitative observation is quantitatively confirmed by the results in Table 9, serving as the empirical foundation for our proposed method.

**Robustness to Diffusion Noise.** As shown in the Noise rows of Table 9, MLLMs exhibit strong stability against diffusive perturbations. We implement noise injection via a diffusion scheduler controlled by a sigmoid function. Despite these perturbations, the Qwen2.5-VL-3B model maintains performance and even achieves a slight average gain of **+0.6%** in general reasoning tasks. Similarly, the 7B model shows negligible performance fluctuations ( $\Delta < 0.3\%$ ) across most benchmarks. This indicates that current MLLMs possess inherent resilience to the high-frequency jitter introduced by the diffusion scheduler, likely due to the robust feature extraction capabilities of the vision encoder.

**Insight I:** This robustness validates the feasibility of our *Noise Consistency* objective. Since the model demonstrates invariance to diffusion noise, explicitly enforcing output consistency between clean and noisy views acts as a safe regularization term. This stabilizes the policy without degrading representation quality.

**SYSTEM:**

You are a helpful assistant.

**USER:**

{question}

You first think through the reasoning process as an internal monologue, enclosed within `<think>` `</think>` tags. Then, provide your final answer enclosed within `\boxed{}`.

Figure 3: The standardized prompt template employed across all training and evaluation phases. To ensure consistent reasoning behaviors and facilitate automated answer extraction, we explicitly instruct the model to encapsulate its chain-of-thought within `<think>` tags and place the final result inside a `\boxed{}` command.

Setting	General Multimodal Reasoning							Medical Multimodal Reasoning				
	Geo3k	Vista	WeMath	MVerse	MVerse-V	MMK12	AVG	Slake	Path	Rad	PMC	AVG
<i>Qwen2.5-VL-3B Backbone</i>												
Original	20.6	40.6	23.9	30.9	28.2	34.8	29.8	48.7	59.2	40.3	46.8	48.8
Noise	22.6 <sub>+2.0</sub>	41.4 <sub>+0.8</sub>	26.5 <sub>+2.6</sub>	30.8 <sub>-0.1</sub>	26.2 <sub>-2.0</sub>	35.1 <sub>+0.3</sub>	30.4 <sub>+0.6</sub>	48.1 <sub>-0.6</sub>	58.5 <sub>-0.7</sub>	40.6 <sub>+0.3</sub>	46.2 <sub>-0.6</sub>	48.4 <sub>-0.4</sub>
Masked	6.2 <sub>-14.4</sub>	24.2 <sub>-16.4</sub>	17.8 <sub>-6.1</sub>	21.5 <sub>-9.4</sub>	16.5 <sub>-11.7</sub>	31.6 <sub>-3.2</sub>	19.6 <sub>-10.2</sub>	31.5 <sub>-17.2</sub>	37.8 <sub>-21.4</sub>	26.2 <sub>-14.1</sub>	29.4 <sub>-17.4</sub>	31.2 <sub>-17.6</sub>
<i>Qwen2.5-VL-7B Backbone</i>												
Original	33.8	55.9	41.8	45.6	36.9	43.7	42.9	63.7	60.6	61.3	52.2	59.5
Noise	30.5 <sub>-3.3</sub>	56.3 <sub>+0.4</sub>	41.6 <sub>-0.2</sub>	44.5 <sub>-1.1</sub>	38.5 <sub>+1.6</sub>	44.6 <sub>+0.9</sub>	42.7 <sub>-0.2</sub>	63.5 <sub>-0.2</sub>	59.8 <sub>-0.8</sub>	61.5 <sub>+0.2</sub>	51.9 <sub>-0.3</sub>	59.2 <sub>-0.3</sub>
Masked	8.0 <sub>-25.8</sub>	32.4 <sub>-23.5</sub>	30.5 <sub>-11.3</sub>	31.2 <sub>-14.4</sub>	23.2 <sub>-13.7</sub>	39.6 <sub>-4.1</sub>	27.5 <sub>-15.4</sub>	42.1 <sub>-21.6</sub>	38.4 <sub>-22.2</sub>	40.5 <sub>-20.8</sub>	33.2 <sub>-19.0</sub>	38.6 <sub>-20.9</sub>

Table 9: Robustness evaluation under visual perturbations. Results are presented as **Accuracy<sub>Difference</sub>**. The difference ( $\Delta$ ) represents the gap compared to the **Original** setting. **Red subscripts** indicate performance gains ( $+\Delta$ ), while **Blue subscripts** indicate drops ( $-\Delta$ ).

**Sensitivity to Semantic Masking.** Conversely, the models demonstrate high sensitivity to patch masking. When a portion of the visual input is occluded, performance degrades sharply. Notably, the 7B model suffers a severe average drop of **–20.9%** in the medical domain and **–15.4%** in general tasks. This degradation is significantly more pronounced than that caused by noise, indicating that reasoning depends heavily on specific visual patches rather than language priors alone.

**Insight II:** This sensitivity confirms that visual tokens are critical for correct reasoning. It motivates employing masking as a challenging view in the reinforcement learning loop. Exposing the policy to masked inputs forces the model to maximize information utilization from the remaining visible patches, thereby reducing hallucination and enhancing the grounding of the reasoning process.

**Summary.** MLLMs process these two perturbations through fundamentally different mechanisms. Diffusion noise acts as a low-level surface artifact to which pre-trained visual encoders exhibit strong

invariance. In contrast, patch masking acts as a high-level semantic disruption that breaks the visual continuity required for logical deduction. This disparity highlights a critical insight: while visual representations are texturally robust, reasoning policies remain fragile to structural incompleteness. *This observation directly underpins our methodology, where we leverage diffusion noise for consistency regularization and masking for hardness-aware policy learning.*

## E RLVR Visual Dependency Experiments

To rigorously investigate whether current RLVR methods genuinely leverage visual information or merely exploit linguistic priors, we conducted a series of *blind experiments*. We maintained the identical training setup as the main experiments, training policies on the VIRC-39K (Wang et al., 2025a) dataset using the standard hyperparameters for both GRPO (Shao et al., 2024) and DAPO (Jiang et al., 2025). We also presented case study comparisons in Section F. During evaluation, we introduced two

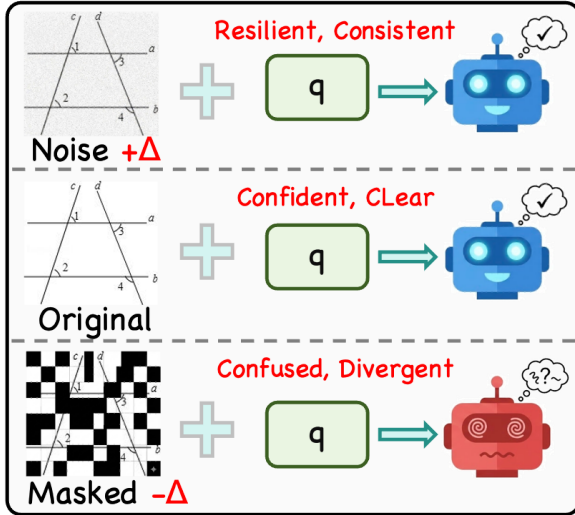


Figure 4: **Visual Dependency Analysis.** Divergence in reasoning paths. Current MLLMs show minimal sensitivity to masked vs. perturbed inputs (consistent in top rows), but become confused when visual semantics are masked (divergent in bottom row), indicating a lack of visual grounding.

modality-blind settings to sever the visual semantic link:

- **Blank Image (B/W):** The original visual input is randomly replaced with a solid black or white image. This removes all visual semantics while preserving the multimodal input structure.
- **Text Only:** The visual tokens are entirely discarded, forcing the model to rely solely on the textual query and its internal parametric knowledge.

**Visual Redundancy in GRPO.** Table 10 presents the comparative performance across six general multimodal reasoning benchmarks. For **GRPO**, removing visual modalities causes a performance decline from 62.0% to 58.3%. However, this drop is disproportionately small given the multimodal nature of these tasks. The fact that the policy retains nearly 94% of its original efficacy in the blind setting indicates that the model treats visual evidence as largely redundant. Rather than grounding reasoning in visual perception, the model relies primarily on linguistic priors and parametric knowledge.

**Visual Interference in DAPO.** In contrast, **DAPO** treats visual input as a distraction. Unexpectedly, ablating visual signals leads to marginal

performance improvements. As shown in Table 10, the Text Only configuration achieves an average accuracy of **56.3%**, outperforming the original multimodal baseline (55.8%). Specifically, on MathVista, replacing informative images with blank frames yields a **+3.5%** gain (61.9%  $\rightarrow$  65.4%), and discarding images boosts performance on PAPO\_MMK12 (Meng et al., 2025b) by **+1.4%**. These results suggest that the current RLVR objective encourages the policy to ignore visual information in favor of statistical language correlations, effectively treating images as noise.

**The Cause: Linguistic Shortcuts.** These blind experiments identify a critical limitation in current multimodal RLVR paradigms. When optimizing solely for outcome-based textual rewards, policies learn to bypass the visual encoder to maximize reward efficiency. Instead of establishing a causal link between perception and reasoning, the model overfits to syntactic patterns in the reasoning chain. This decoupling leads to hallucinations, where the model generates coherent rationales that are detached from the actual visual input.

**Insight: Enforcing Visual Dependency.** These findings motivate our proposed framework. Scaling reinforcement learning on multimodal data is insufficient if the optimization does not explicitly penalize the bypass of visual information. Our **DVRP** framework addresses this by introducing a visual triplet constraint. By maximizing divergence on masked inputs (Sensitivity) and minimizing it on perturbed inputs (Robustness), DVRP ensures the policy treats visual tokens as necessary conditions for reasoning. This mechanism re-couples perception and reasoning, ensuring that performance gains derive from genuine visual comprehension rather than linguistic shortcuts.

## F Qualitative Analysis of Visual Dependency

To understand the *visual bypass* phenomenon observed in Section E, we qualitatively examine the reasoning trajectories of the **DAPO** policy under three inference settings: *Text-Only*, *Blank Image*, and the *Standard* (Original Image) setting. Due to space constraints, the displayed CoT rollouts have been streamlined using Gemini-3-Pro to ensure conciseness while strictly preserving the original logical flow and specific errors. We focus on cases where visual information is theoretically essential

Method & Setting	General Multimodal Reasoning Benchmarks						
	Geo3k	Vista	WeMath	MVerse	MVer-V	MMK12	AVG
<b>Base Model</b> (Qwen2.5-VL-7B)	33.8	55.9	41.8	45.6	36.9	43.7	43.0
<b>GRPO Policy</b> (Original)	40.2	65.5	66.1	66.5	61.7	72.1	62.0
w/ Black/White Image	37.8 <sub>-2.4</sub>	64.8 <sub>-0.7</sub>	65.2 <sub>-0.9</sub>	64.2 <sub>-2.3</sub>	60.3 <sub>-1.4</sub>	66.6 <sub>-5.5</sub>	59.8 <sub>-2.2</sub>
w/ Text Only Input	34.1 <sub>-6.1</sub>	34.1 <sub>-3.5</sub>	63.1 <sub>-3.0</sub>	63.2 <sub>-3.3</sub>	61.1 <sub>-0.6</sub>	66.5 <sub>-5.6</sub>	58.3 <sub>-3.7</sub>
<b>DAPO Policy</b> (Original)	35.9	61.9	58.5	55.6	51.0	71.9	55.8
w/ Black/White Image	34.9 <sub>-1.0</sub>	65.4 <sub>+3.5</sub>	58.1 <sub>-0.4</sub>	54.2 <sub>-1.4</sub>	51.3 <sub>+0.3</sub>	68.2 <sub>-3.7</sub>	55.4 <sub>-0.4</sub>
w/ Text Only Input	34.6 <sub>-1.3</sub>	62.5 <sub>+0.6</sub>	57.4 <sub>-1.1</sub>	55.2 <sub>-0.4</sub>	54.5 <sub>+3.5</sub>	73.3 <sub>+1.4</sub>	56.3 <sub>+0.5</sub>

Table 10: Ablation study on visual dependency. We compare the performance stability of GRPO and DAPO under **Black/White Image** (texture-only) and **Text Only** (blind) settings. The **Base Model** serves as the zero-shot baseline. For GRPO and DAPO (highlighted in blue), the subscripts denote the performance gap ( $\Delta$ ) relative to their respective **Original** settings. Note that DAPO shows counter-intuitive gains in “Text Only” mode (indicated by red subscripts), suggesting a potential bias towards linguistic shortcuts.

for deduction. As shown in the examples below, the policy frequently arrives at the correct solution in the blind settings (Text-Only and Blank Image) by *hallucinating* specific visual values or exploiting linguistic artifacts in the questions. This qualitative evidence confirms that the model often treats visual data as redundant, achieving high rewards through spurious shortcuts rather than genuine multimodal comprehension.

**GEOMETRY3K**

**Question:**  
Find x.

**GT Answer:**  
8

**Text-Only Policy (No Vision)**

Use tangent definition:  $\tan(60^\circ) = \text{opp}/\text{adj} = y/x = \sqrt{3}$ . Finding x... use cosine:  $\cos(60^\circ) = x/y = 1/2$ . Also sine:  $\sin(60^\circ) = 8\sqrt{3}/y = \sqrt{3}/2$ . [Hallucinated  $8\sqrt{3}$  from nowhere]

Answer: 8 ✓

**Blank Image Policy (Visual Noise)**

$\tan(60^\circ) = y/(8\sqrt{3}) = \sqrt{3}$ . Need adjacent x:  $\cos(60^\circ) = x/y = 1/2$ . Derive  $y = 8\sqrt{3}/\cos(60^\circ) = 16\sqrt{3}$ . Use Pythagoras:  $y^2 = x^2 + (8\sqrt{3})^2$ . [Confused derivation]

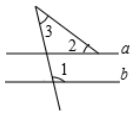
Answer: 8 ✓

**Original Policy (DAPO - Ours)**

Identify 30-60-90 triangle. Side opposite  $30^\circ$  is shortest; opposite  $60^\circ$  is x; hypotenuse is  $2 \times$  shortest. Wait, from diagram: side opp  $60^\circ$  is x, side opp  $30^\circ$  is  $8\sqrt{3}$ . Using ratio  $1 : \sqrt{3}$ ,  $x = 8\sqrt{3}/\sqrt{3} = 8$ .

Answer: 8 ✓

## MATHVERSE



**Question:**  
 $a \parallel b$ ,  $\angle 2 = 35^\circ$ ,  $\angle 3 = 40^\circ$ . Find  $\angle 1$ .

**GT Answer:**  
 B (105°)

### Text-Only Policy (No Vision)

Since  $a \parallel b$  and  $\angle 2 = 35^\circ$ , then  $\angle AEC = 35^\circ$ .  $\angle 1 = \angle AEC + \angle 3 = 35^\circ + 40^\circ = 75^\circ$ . [Geometric Logic Failure]

Answer: B ✓

### Blank Image Policy (Visual Noise)

Angle 4 corresponds to Angle 3, so Angle 4 = 40.0. Angle 1 is on straight line:  $180^\circ - \text{Angle } 2 - \text{Angle } 4 = 180^\circ - 35^\circ - 40^\circ = 105^\circ$ . [Correct logic by chance]

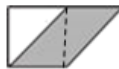
Answer: B ✓

### Original Policy (DAPO - Ours)

Since  $a \parallel b$ , Angle 4 (alternate interior) = Angle 3 = 40.0. Angle 1, 2, and 4 form a straight angle.  $\angle 1 = 180^\circ - 35.0 - 40.0 = 105.0$ .

Answer: B ✓

## WE-MATH



### Question:

Square perimeter 20 → side 5. Area of shaded parallelogram?

**GT Answer:**  
 D (25)

### Text-Only Policy (No Vision)

Perimeter 20 → side 5. Shaded area is two triangles forming half square?  $25/2 = 12.5$ ? Options don't match. Re-evaluating: assume standard problem setup where shaded = full area or options imply 25. Choosing D.

Answer: D ✓

### Blank Image Policy (Visual Noise)

Perimeter 20 → side 5. Parallelogram base = side = 5. Height = side = 5. Area = base × height =  $5 \times 5 = 25$ .

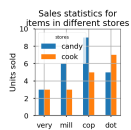
Answer: D ✓

### Original Policy (DAPO - Ours)

Perimeter 20 → side 5. Visual confirmation: Shaded parallelogram spans full base and height of the square. Area =  $5 \times 5 = 25$ .

Answer: D ✓

## MATHVISTA



**Question:**  
 Items sold < 5 units in at least one store?

**GT Answer:**  
 2

### Text-Only Policy (No Vision)

"Very": both < 5. "Mill": candy 6 (no), cook 3 (<5) → fails 'at least one'? Logic error. "Cop": candy 9, cook 5. "Dot": 5 and 7. [Hallucinated numbers]

Answer: 2 ✓

### Blank Image Policy (Visual Noise)

"Very": both 3. "Mill": candy 6, cook 3. "Cop": candy 9, cook 5. "Dot": candy 5, cook 7. [Identical Hallucination to Text-Only]

Answer: 2 ✓

### Original Policy (DAPO - Ours)

Reading chart: "Very" (both bars 3, <5), "Mill" (Candy 6, Cook 3 <5), "Cop" (Candy 9, Cook 5), "Dot" (Candy 5, Cook 7). Only Very and Mill satisfy condition.

Answer: 2 ✓

## PAPO-MMK12



### Question:

Ammonia synthesis  $\Delta H < 0$ . Which statement is incorrect?

**GT Answer:**  
 A

### Text-Only Policy (No Vision)

A. Incorrect. Exothermic reaction ( $\Delta H < 0$ ): high temp shifts equilibrium left (lower yield), though it improves rate. B. Correct: Pressure increases rate. C. Correct: Catalyst lowers activation energy. D. Correct: Separating  $NH_3$  shifts equilibrium forward.

Answer: A ✓

### Blank Image Policy (Visual Noise)

A. Incorrect.  $\Delta H < 0$  means exothermic. Increasing temp shifts equilibrium left (Le Chatelier), decreasing conversion. High temp is for kinetics, not yield. B, C, D are standard correct statements.

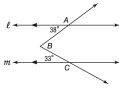
Answer: A ✓

### Original Policy (DAPO - Ours)

A. Incorrect. High temp helps activation energy but is unfavorable for exothermic equilibrium yield. It's a compromise. B. Correct: Pressure increases rate (conc. increases). C. Correct: Catalyst lowers barrier. D. Correct: Mass action law.

Answer: A ✓

**MATHVERSE-  
VIS**



**Question:**  $l \parallel m$ . Find  $\angle ABC$ .

**GT Answer:** D (71)

**Text-Only Policy (No Vision)**

$l \parallel m$ , transversal  $AB \rightarrow \angle BAC = 38^\circ$ . Sum of angles in  $\triangle ABC$ :  $\angle ABC + 38^\circ + \dots = 71^\circ$ ? (Hallucinated calculation to match options).

Answer: D ✓

**Blank Image Policy (Visual Noise)**

$\angle BAC = 38^\circ$  (alternate interior).  $\angle ACB$  supplementary to 33? No. Calculation:  $38 - 33 = 5^\circ$ . [Hallucinated subtraction logic]

Answer: D ✓

**Original Policy (DAPO - Ours)**

Use Exterior Angle Theorem.  $\angle BAC$  is exterior to  $\triangle ABC$ ? No, diagram shows transversal. Logic:  $180 - 38 = 142$ . Exterior angle summation:  $38^\circ + 33^\circ = 71^\circ$ .

Answer: D ✓

## G Qualitative Comparison of RLVR Algorithms

In this section, we present a comparative case study of reasoning trajectories generated by the GRPO baseline (Shao et al., 2024), the DAPO method (Yu et al., 2025), and our proposed DVRP-D framework. Due to space constraints, the displayed CoT rollouts have been streamlined using Gemini-3-Pro. This process ensures conciseness while strictly preserving the original logical flow and specific errors.

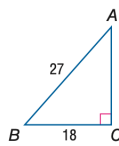
**Evaluation Methodology.** To conduct a rigorous qualitative assessment, we randomly sampled **50 distinct cases** spanning six diverse math reasoning datasets. We employed Gemini-3-Pro as an external evaluator to assess the quality of reasoning chains based on two primary criteria: *visual faithfulness* and *logical consistency*. The evaluation specifically focuses on identifying instances where the model generates plausible text that contradicts visual facts (hallucination) or ignores critical visual cues (blind reasoning).

**Analysis of Baselines.** The comparative analysis of these sampled cases reveals that baselines frequently suffer from perception-reasoning decoupling, manifesting in distinct failure modes. GRPO tends to exhibit **visual hallucinations**, such as describing incorrect object colors or counts to force

a logical conclusion. It also suffers from **option mapping failures**, where valid intermediate calculations inexplicably lead to incorrect multiple-choice selections. Similarly, while DAPO follows a structured format, it frequently demonstrates **logical inconsistencies** and **visual misalignment**. Specific errors include failing numerical comparators despite accurate counting (e.g., concluding  $2 < 4$  is false) or misinterpreting graph trends (e.g., confusing exponential growth with linear relationships). These patterns indicate that baseline reasoning paths often diverge from visual reality due to an over-reliance on linguistic priors.

**Efficacy of DVRP-D.** In contrast, the evaluation confirms that DVRP-D demonstrates superior *visual grounding*. Our method effectively anchors reasoning steps to specific visual evidence. Crucially, the assessment highlights that DVRP-D exhibits distinct self-correction behaviors. It actively verifies visual features during intermediate steps and adjusts its reasoning when initial assumptions conflict with visual observation. This mechanism significantly reduces the occurrence of ungrounded hallucinations and ensures that the final answer is causally derived from the visual input.

**GEOMETRY3K**



**Question:** Find  $\angle A$  to nearest tenth.

**GT Answer:** 41.8

**GRPO (Baseline)**

$\dots \tan(\angle A) = \frac{18}{9\sqrt{5}} = \frac{2}{3}$ . No.  $\tan^{-1}(2/3) \approx 33.7^\circ$ . Incorrectly simplifies the fraction, leading to wrong angle.

Answer: 33.7 ✗

**DAPO (Baseline)**

$\dots AC = 9\sqrt{5}$ .  $\tan(\angle A) \approx 0.8944$ .  $\tan^{-1}(0.8944) \approx 41.4^\circ$ . Correct approach but fails at final precision/rounding step.

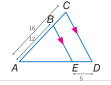
Answer: 41.4 ✗

**DVRP-D (Ours)**

Pythagoras:  $AC = 9\sqrt{5}$ .  $\tan(\angle A) = \frac{2\sqrt{5}}{5}$ . Result  $\approx 41.8^\circ$ . Correct geometric derivation and calculation.

Answer: 41.8 ✓

## MATHVERSE



**Question:**  
BE  $\parallel$  CD. Find AE. (A:10, B:12, C:15, D:16)

**GT Answer:**  
C

### GRPO (Baseline)

Similarity ratio  $12/16 = AE/(AE + 5)$ .  $12AE + 60 = 16AE \rightarrow AE = 15$ .

Calculates 15 correctly, but hallucinates selecting option A.

**Answer:**  A ×

### DAPO (Baseline)

Proportion  $\frac{12}{16} = \frac{AE}{AE + 5}$ . Solving gives  $AE = 15$ .

Correct calculation, but fails to map result to option C.

**Answer:**  A ×

## MATHVISTA



**Question:**  
Is count(front fighter) < count(behind bus)?

**GT Answer:**  
Yes

### GRPO (Baseline)

Front: Blue van, Bus (2 objects). Behind: Yellow van, Plane, Bus, Bicycle (4 objects).  $2 < 4$ ? No.

Correct counting, but logical comparator failure ( $2 < 4$  is True).

**Answer:**  No ×

### DAPO (Baseline)

Front: 2 objects. Behind: 4 objects. Conclusion: No.

Identical logical failure; fails to evaluate inequality correctly.

**Answer:**  No ×

### DVRP-D (Ours)

Behind bus: Yellow van, airplane, bus, bicycle (4 items). Comparison validates condition.

Correctly counts and executes logical comparison.

**Answer:**  Yes ✓

## WE-MATH



### GRPO (Baseline)

Blackboard ①... upper half contains two white squares.

Visual hallucination; describes wrong object/color.

**Answer:**  C ×

### GT Answer:

B

### DAPO (Baseline)

Observing upper half... Blackboard ① has three yellow squares? No, concludes C (White).

Conflicted reasoning leading to hallucinated choice.

**Answer:**  C ×

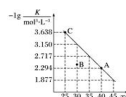
### DVRP-D (Ours)

Focus on Blackboard ①. Upper half contains yellow squares. Count is 3.

Accurate visual grounding and attribute recognition.

**Answer:**  B ✓

## PAPO-MMK12



### GRPO (Baseline)

Analyzes D:  $v_{fwd} > v_{rev}$ . Concludes D is incorrect.

Misinterprets the kinetic state at point B.

**Answer:**  D ×

### DAPO (Baseline)

Analyzes B: Volume fraction unchanged means equilibrium (Correct). Analyzes D... finds D incorrect.

Correctly identifies B is true, but mistakenly targets D as answer.

**Answer:**  D ×

### DVRP-D (Ours)

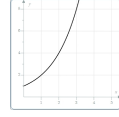
Endothermic reaction ( $K$  increases with  $T$ ). Statement B (vol fraction) implies equilibrium... B is the answer.

Correctly identifies the target statement.

**Answer:**  B ✓

## MATHVERSE- VIS

Consider the graph given.  
Which of the following relationships could be  
represented by the graph?  
Options:  
A) The number of handshakes,  $y$ , made by  $x$  people in  
a room if every person shakes hands with every  
other person.  
B) The area,  $y$ , of a  $100 \times 100$  mm square piece of paper being folded in half  $x$   
times.  
C) The number of participants,  $y$ , in a  
pentadecade conference when there are  $x$  panellists  
speaking in 2 sessions.



### Question:

Identify the graph relationship (Linear, Exp, Quad).

**GT Answer:**  
B

### GRPO (Baseline)

$x = 1, y = 1 \dots x = 5, y = 31$ . Matches  $y = x(x - 1)/2$ ? (Quadratic).

Fails to fit data points to correct function class.

**Answer:**  A

### DAPO (Baseline)

$y = 3x$ ? Linear relationship matches graph?

Severe visual misalignment; interprets curve as linear.

**Answer:**  C

### DVRP-D (Ours)

Rapid increase.  $x = 5, y \approx 31$ . Matches  $y = 2^x$  (Exponential).

Correctly recognizes exponential growth pattern from plot.

**Answer:**  B